Reviews

Structures of large transition metal clusters

O. A. Belyakova and Yu. L. Slovokhotov[★]

*A. N. Nesmeyanov Institute of Organoelement Compounds, Russian Academy of Sciences,
28 ul. Vavilova, 119991 Moscow, Russian Federation.
Fax: +7 (095) 135 5085. E-mail: slov@ineos.ac.ru*

The present review surveys the results of X-ray diffraction studies of large stoichiometric transition metal clusters containing from 20 to 145 atoms in metal cores surrounded by ligand shells (72 compounds). Structures of such clusters have fragments of close packings (face-centered cubic (f.c.c.), hexagonal close (h.c.p.), and body-centered cubic (b.c.c.) packings) characteristic of crystalline bulk metals as well as mixed packings (f.c.c./h.c.p.), local close packings with pentagonal symmetry, and strongly distorted "amorphous" packings. The obseved packing types, their distortions, and the relationship between the atomic structures of metal cores and the atomic radial distribution functions (RDF) are discussed. The structural principles established for the large clusters are applied to analysis of the experimental RDF for metal nanoparticles determined by X-ray diffraction and EXAFS spectroscopy.

Key words: large metal clusters, X-ray diffraction analysis, atomic packing, atomic radial distribution, nanoparticles.

1. Introduction

Clusters are compact stable atomic groups in which the shortest interatomic distances are of the order of the sums of atomic radii. Clusters can either be isolated or interact with each other directly or through intermediate atoms in the condensed phase. Substances consisting of clusters are referred to as cluster compounds. More complicated composites of substances containing clusters are called cluster materials.

Transition metal clusters have attracted considerable attention over the last half century. This interest is associated with the use of these compounds, primarily, in ca-talysis[1,2] as well as for the preparation of materials with unique magnetic properties[3—5] and the design of devices in nanoelectronics at the molecular level.[6] Theorists focus their research on the physicochemical properties[7] and electronic and atomic structures[8,9] of these compounds.

Naked ligand-free clusters occur in some main-group metal compounds (for example, the Zintl phases[10]). The M_{12} clusters are present in crystalline α-boron and a number of borides.[11] Extended isolated fragments consisting of metal atoms are typical, in particular, of mercury compounds.[12] True ligand-free clusters isolated from each other are generated by condensation of metal vapors *in vacuo* or in a cryomatrix.[13] Inert gas clusters formed upon

gas expansion into a vacuum can be considered as structural prototypes of the above ligand-free clusters. Theoretical and experimental structural studies of such Lennard-Jones clusters[14−17] revealed the characteristic structural features applicable also to metal clusters with ligands.

Stable transition metal clusters always have a ligand environment. In this case, the M_n group is called a "metal core" or "cluster core." The size of the metal core in clusters can vary from several angstroms to hundreds of nanometers,[18] and the clusters can contain from a few atoms up to 10^9-10^{10} atoms. Both homo- and hetero-metallic clusters are known. Bimetallic clusters of sizes starting with several nanometers are called alloy particles, whose possible compositions differ substantially from those of bulk alloys.[19,20] Bimetallic clusters consisting of transition and main-group elements pass continuously into clusters of binary compounds A_nB_m as the differences in their atomic radii and electronegativities increase.

From the viewpoint of electronic structures, clusters are intermediate between mononuclear coordination compounds, which possess localized electronic systems with discrete energy levels, and bulk metals, which have delocalized electronic systems consisting of broad energy bands. As the number of metal atoms in the cluster increases, the number of bonding and antibonding electronic levels increases (which, in the limit, form the valence and conduction bands, respectively), whereas the energy gap between the electronic levels decreases (Fig. 1). Cluster compounds can exhibit properties typical of metals, such as paramagnetism and conductivity.

The changes in the electronic structure of the cluster as a function of its size are called the quantum size effect.[6a,b] In the modern materials science, metal and

binary cores of sizes up to several tens of nanometers that are present in cluster materials are called quantum dots. The electronic system of such clusters, which can be composed of tens of thousands of atoms, contains discrete levels; transitions between adjacent levels of a quantum dot are accompanied by photon absorption (emission) in the visible and infra-red spectral regions. Such systems are extensively studied as prototypes of new electrical, magnetic, and optical materials.[21]

Depending on the size of the metal core, clusters can be divided into small, medium-sized, large, and giant clusters.[18] Small clusters of sizes up to 0.5 nm contain 2—6 metal atoms. Medium-sized clusters of sizes of about 0.5 nm can consist of up to 15—20 metal atoms. Large clusters of sizes of ~1 nm contain from several tens to 100—200 metal atoms. Giant clusters or nanoparticles with a diameter of 2—10 nm occurring in some colloidal metals can contain from several hundreds to hundreds of thousands of atoms. This series is concluded with large nanoparticles of sizes larger than 10 nm (10^6-10^{10} atoms) and, finally, bulk metals. The sizes of mosaicity domains in bulk metal crystals approximately correspond to large nanoparticles.

The classification of clusters according to their diameter is rather arbitrary because qualitative changes in the metallic properties in a series of clusters can also be determined by the structure of their metal cores, *i.e.*, by the packing of metal atoms and the fraction of interstitial atoms in the cluster core M_n. From this standpoint, metal cores, which are characterized by a close flexible atomic packing and contain at least one interstitial metal atom, can be considered as large clusters.[22] The total number of atoms in some of such M_n clusters can be smaller than 20 (metal-centered clusters with $n = 12-13$ are known).[23,24] At the same time, a number of knwon clusters with $n > 20$ contain no interstitial metal atoms (see below). In the present review, all metal cores starting with M_{20} are formally classified as large clusters (discussion is extended to some of their analogs with $n < 20$) because their structures are strongly influenced by the atomic packing.

The relationship between the physical and chemical properties of homonuclear clusters, on the one hand, and the properties of the corresponding compact metal, on the other hand, is determined by both the size of the metal core and the nature of the ligand shell. However, in a number of studies, it was stated that the ligand environment has a substantial effect only on the outer atoms on the cluster surface, whereas the manifestation of metallic properties is associated with the presence of interstitial metal atoms surrounded only by other metal atoms.[6a] For example, according to the data from Mössbauer spectroscopy, the chemical shifts of 42 outer Au atoms in the $Au_{55}(PPh_3)_{12}Cl_6$ cluster differ substantially from those of 13 interstitial Au atoms.[25] The Pt_{309} and Pd_{561} clusters in which about one-half of all metal atoms are interstitial
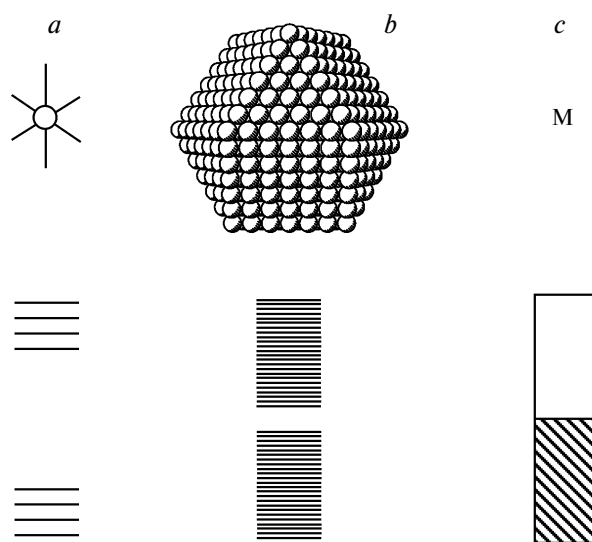
Fig. 1. Schematic representation of electronic levels in (*a*) mononuclear complex, (*b*) large cluster, and (*c*) bulk metal M.

(see Sections 2 and 4) exhibit, to a large extent, properties of bulk metals (magnetic susceptibility, ^{195}Pt NMR, temperature dependence of the heat capacity near 0 K).[6,26]

The physical properties of compounds consisting of either large metal clusters or small metal nanoparticles with a diameter of 1—5 nm depend substantially on the nature of the metal atoms and the type of atomic packing, which are together responsible for the electronic structure of the metal core. Since the atomic packing in such clusters is very flexible and can, for example, be modified by a ligand shell,[22] analysis of the atomic packing is of considerable importance for the discussion of the properties of cluster compounds.

Large metal clusters belong to a unique class of compounds, whose stoichiometry and atomic structures can be exactly determined, although they already contain some features of metal structures and exhibit some metallic properties. As the size of the cluster increases further, it becomes more difficult to achieve a true monodisperse composition and structure distribution within the sample, and the dependence of the physicochemical properties of the substance on the size of the metal core becomes smoother.

In the present review, we focus on the cluster compounds, whose structures were unambiguously established by single-crystal X-ray diffraction study. The principles underlying the structures of the clusters are briefly surveyed in Section 2. The types of atomic packing in large clusters and their relationship with the structures of metal crystal lattices are analyzed in Section 3. Selected results of structural studies of giant clusters[6b] (small nanoparticles) are presented in Section 4. For such giant clusters, the structures of large clusters established by X-ray diffraction analysis serve as a base for the interpretation of the results of other physical methods.

2. Principles of atomic structures of clusters

Although the metal cores of large clusters can sometimes be represented as fragments of metal crystal lattices, in the general case, the observed geometry of the cluster corresponds to the minimum of the total energy of the metal atoms inside the cluster (which tend to form the maximum number of binding interatomic contacts, *i.e.*, to form closest packings) and coordinatively unsaturated surface atoms, which are generally coordinated by ligands. The balance between the number of low-energy interstitial atoms and the number of higher-energy outer atoms on the surface of the metal core is responsible for the above-mentioned flexibility of atomic packings in the clusters. The tendency to an increase in the total number of bonds between atoms in naked clusters determines a compact spheroidal shape of their atomic cores (molecular analog of surface tension). The ligand shell has an oppo-
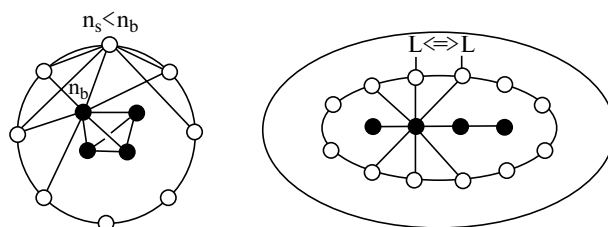

Fig. 2. Schematic representation of a ligand-free cluster containing atoms on the surface and inside the polyhedron (corresponding coordination numbers n_b and n_s are given) and a cluster within a ligand shell.

site effect on the cluster structure; that is, it stabilizes atoms on ist surface (*i.e.*, decreases the "surface tension") and can facilitate an increase in their fraction in the polyhedron due to steric repulsions between the ligands (Fig. 2). A combined effect of the above two factors is responsible for the observed diversity of cluster structures.

The basic principles of structures of large stoichiometric clusters, which were formulated for the first time in the late 1970s by P. Chini,[22] include the electronic saturation of the metal core, the close atomic packing in this core, and the ability of the cluster core to undergo rearrangements induced by small changes in the stoichiometric composition or replacements in the ligand shell. The electronic saturation of the metal core for small clusters is reflected in the rule of magic numbers of valence electrons in stable cluster polyhedra (48 in the triangle M_3, 60 in the tetrahedron M_4, 86 in the octahedron M_6, *etc.*). The rule of magic numbers for clusters with delocalized bonds was suggested in 1970s by K. Wade[27,28] and other authors.[9,29,30] As the number of atoms in the cluster increases, the rule of magic numbers becomes less valid, and it is not fulfilled for large clusters,[31] which is indicative of a transition from the molecular type of bonding in the cluster to the metallic bonding. However, the electronic saturation is approximately retained in large clusters having a small number of unoccupied electronic levels with similar energies above the Fermi level.[32] In this respect, large clusters with a ligand shell are molecular analogs of narrow bandgap semiconductors due to which they are applicable, for example, as quantum materials (see Fig. 1).

In the discussion of the geometry of large clusters, the notions of v_n polyhedra ("polyhedra with *n*-frequency edges") and multi-shell onion-type polyhedra are used. In the v_n polyhedron, *n* corresponds to the number of parts into which each edge of the polyhedron is divided by the atoms located on this edge. For example, a v_3-triangular cluster is derived from a usual triangle by dividing each edge into three parts and, hence, it contains 10 metal atoms one of which occupies the center of the triangle (Fig. 3, *a*). In v_n tetrahedra and v_n octahedra, each face is a v_n triangle (see Fig. 3, *b*). A multi-shell cluster consists
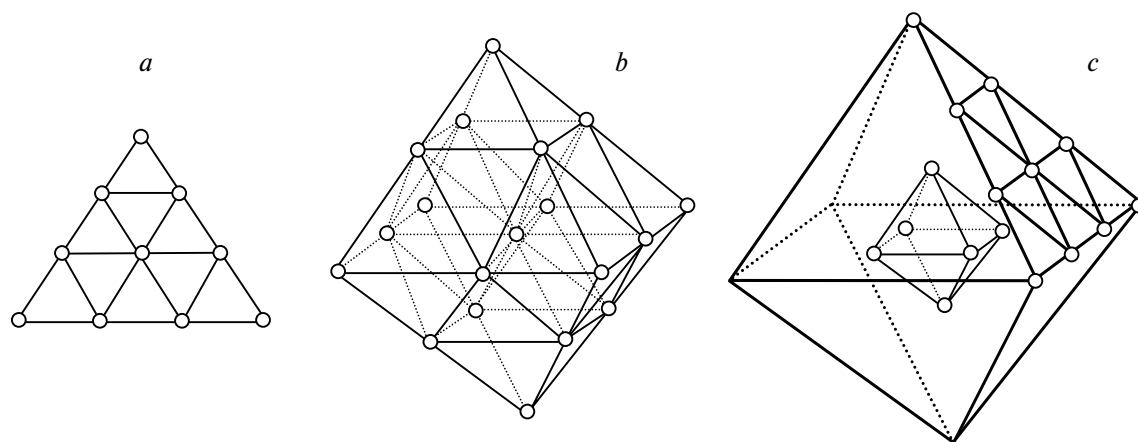
Fig. 3. Idealized polyhedra used for the description of large clusters: (*a*) v_3 triangle; (*b*) centered v_2 octahedron; (*c*) two-shell octahedron (inner v_1 octahedron in the v_3-octahedral shell); the arrangement of atoms on one face of the v_3 octahedron is shown.

of the central atom surrounded by k nested coordination spheres (see Fig. 3, *c*). For instance, a two-shell icosahedron and cuboctahedron are formed by the central M atom, the first coordination sphere consisting of 12 M atoms, and the second sphere of 42 M atoms surrounding the first sphere. The k-th sphere around the central atom in the icosahedral and cuboctahedral clusters contains the magic number* $(10k^2 + 2)$ of metal atoms.

The standard geometric parameters of molecules (bond lengths, bond angles, torsion angles, *etc*.), which are determined from X-ray diffraction data for low-molecular-weight compounds, are less informative for large clusters in which they can vary within a broad range. The type of atomic packing in the cluster core is the most important overall parameter of this class of compounds. For compounds with known structures, this packing, which is directly related to the electronic structure and, consequently, to the physical characteristics of the cluster, can be determined both at the qualitative level (based on the shape of the polyhedron formed by the closest local environment of the interstitial metal atoms) and semiquantitatively (from histograms of interatomic distances). The atomic packing correlates with the overall shape of the metal core only in a few large high-symmetry clusters.

Almost all large clusters studied by single-crystal X-ray diffraction are formed by late transition metals (Table 1). Their structures often contain fragments of packings typical of crystalline metals: the face-centered cubic (f.c.c.) and hexagonal close (h.c.p.) packings as well as the body-centered cubic (b.c.c.) packing, whose density is close to those of the first two packings. In ideal crystallographic packings, the environment of each atom involves an integer number of adjacent atoms located at a strict distance. For instance, in the face-centered cubic packing with the shortest interatomic distance a, the numbers of atoms

---

* The magic numbers according to P. Chini's classification[22] are used.

Table 1. Shortest interatomic distances (*d*) and packing modes in bulk crystalline metals (M) that form large clusters (296 K)[33]

M	d/Å	Packing mode	M	d/Å	Packing mode
Fe	2.482	b.c.c.	Ag	2.889	f.c.c.
Co	2.506	h.c.p.	Re	2.741	h.c.p.
Ni	2.492	f.c.c.	Os	2.675	h.c.p.
Cu	2.556	f.c.c.	Ir	2.715	f.c.c.
Ru	2.650	h.c.p.	Pt	2.775	f.c.c.
Rh	2.690	f.c.c.	Au	2.884	f.c.c.
Pd	2.751	f.c.c.			

located at distances R are 12 ($R = a$), 6 ($R = a\sqrt{2}$), 24 ($R = a\sqrt{3}$), 12 ($R = 2a$), *etc*.[34] The standard distances (in dimensionless units a/R) and the coordination numbers in the f.c.c., h.c.p., and b.c.c. packings along with the symmetry of the local environments in these packings are given in Table 2.

For finite-size clusters, the histogram of interatomic distances can be calculated from the atomic coordinates of the crystal structure. The positions of the maxima in this histogram can be compared with those characteristic of ideal packings. This approach enables one to unambiguously reveal the packing type in clusters with a rather small (0.1—0.2 Å) dispersion of interatomic distances around the maxima of the atomic radial distribution function (RDF). More substantial distortions of the atomic packing lead to broadening and coalescence of maxima in the histograms.

One-dimensional radial distribution histograms serve as a helpful, although still little used, way of describing complicated cluster structures.* A comparison of these histograms calculated for stoichiometric clusters, whose

---

* In recent years, two-dimensional polar diagrams have been suggested to be used for the characterization of complicated and distorted packings.[35]

Table 2. Coordination spheres in main close packings[34]

f.c.c. (O_h)		h.c.p. (D_{3h})		b.c.c. (O_h)	
R/a*	N	R/a	N	R/a	N
1	12	1	12	1	8
$\sqrt{2}$	6	$\sqrt{2}$	6		
				$\sqrt{(4/3)}$	6
$\sqrt{3}$	24	$\sqrt{(8/3)}$	2	$\sqrt{(8/3)}$	12
		$\sqrt{3}$	18		
		$\sqrt{(11/3)}$	12	$\sqrt{(11/3)}$	24
2	12	2	6	2	8
$\sqrt{5}$	24	$\sqrt{5}$	12		
				$\sqrt{(16/3)}$	6
		$\sqrt{(17/3)}$	12		
$\sqrt{6}$	8	$\sqrt{6}$	6		
		$\sqrt{(19/3)}$	6	$\sqrt{(19/3)}$	24
		$\sqrt{(20/3)}$	12	$\sqrt{(20/3)}$	24
$\sqrt{7}$	48	$\sqrt{7}$	24		
		$\sqrt{(22/3)}$	6		
$\sqrt{8}$	6			$\sqrt{8}$	24
		$\sqrt{(25/3)}$	12		
3	36	3	12	3	8

* R is the distance to the atoms of the coordination sphere; a is the shortest interatomic distance.

atomic structures are known, with the experimental RDF determined by other methods (X-ray and electron diffraction, EXAFS spectroscopy) for nonstoichiometric cluster compounds is of particular importance.

In finite-size clusters, a close icosahedral atomic packing without substantial distortions of the shortest interatomic distances can occur.[36] Such local close packings, which cannot exist in crystal lattices, are called packings of "soft spheres," whose diameters can increase or decrease providing a relaxation of mechanical stresses. In phases of crystalline metals, an icosahedral environment can be present only as twinning defects, whereas such an environment is often observed in large clusters. The structures of icosahedral clusters hve been considered in detail, for example, in the recent review.[37]

In addition to large metal clusters, a series of large binary and quasibinary clusters containing nonmetal atoms were studied by single-crystal X-ray diffraction in the last decades. Among the latter are $Cu_{146}Se_{73}(PPh_3)_{30}$ (containing a flattened cluster core characterized by the maximum size of ~4 nm),[38] $Ag_{124}Se_{57}(SePBu^t_2)_4Cl_6(diphos^*)_{12}$ (diphos* is $Bu^t_2P(CH_2)_5PBu^t_2$) containing the quasispherical core with a diameter of ~3 nm,[39] or large Mo and W polyoxo anions, which also contain more than 100 metal atoms in the metal oxide polyhedron (for example, the structure of $Na_{48}[H_xMo_{368}O_{1032}(H_2O)_{240}(SO_4)_{48}] \cdot yH_2O$ studied recently contains $y \approx 1000$ water molecules inside the extended metal oxide shell with a length of ~6 nm [40]). All these clusters, which can be described as fragments of the crystalline binary compounds M_nX_m (X are nonmetal atoms), are beyond the scope of the present review.

Large metal clusters whose structures were established by single-crystal X-ray diffraction are listed in Table 3.* We chose the clusters based on the formal criterion, *viz.*, the presence of at least 20 metal atoms in the core (see the Introduction). In this case, a number of clusters with smaller metal cores, which already contain interstitial metal atoms (for example, $[Rh_{13}H_x(CO)_{24}]^{(5-x)-}$ with the structure of a metal-centered twinned cuboctahedron[24]), were ignored. Besides, the metal cores of some clusters containing more than 20 metal atoms, in particular, the metal cores of the $[Os_{18}Hg_2(CO)_{42}C_2]^{4-}$,[44] $[Os_{18}Hg_2(CO)_{40}C_2]^{2-}$,[45] $\{[Os_{10}(CO)_{24}C]_2Hg\}^{2-}$,[46] $Os_{12}Rh_9(CO)_{44}Cl$,[49] and $[Ru_{20}Cu_6(CO)_{48}H_4Cl_2]^{4-}$ clusters[70] (which are composed of several small or medium-sized polyhedra linked to each other) cannot be assigned to a particular packing mode (see Table 3). Their structures are also not discussed in our review.

X-ray diffraction data for compounds of this type are scarce because of the difficulties associated with the synthesis and isolation of large metal clusters in the individual form. Systematic studies of large stoichiometric clusters are carried out only by a few research groups throughout the world. Among them, the laboratory headed by Lawrence F. Dahl at the Madison University (USA) is by far a leading team both as regards the scope of research and actual achievements. In this laboratory, the largest known metal clusters have been synthesized and characterized by X-ray diffraction. Table 3 presents the chemical composition, the diameter of the metal core D (estimated from the distance between the two most remote atoms), and the mode of atomic packing for each cluster as well as the references to the corresponding papers. The parameter N is the number of atoms involved in the metal core of the cluster. For clusters containing exopolyhedral metal atoms (which are not directly linked to the cluster core by metal—metal bonds), N is smaller than the total number of the metal atoms in the chemical formula. It should be noted that in most of the clusters, the hydride atoms detected by IR and NMR spectroscopy were not revealed by X-ray diffraction due to their small scattering power and, generally, strong X-ray absorption by single crystals with a high metal content. For the same reasons, in some clusters of heavy elements, the compositions and

---

* We used the Cambridge Structural Database (CSD) as well as selected original studies and abstracts of papers. For compounds stored in the CSD, the complete structural data, including the atomic coordinates in the unit cell, are available. For these compounds (see Table 3), the references to the published data along with their six-letter CSD refcodes are given. When the original studies or abstracts of papers were used as a source of information, the cluster structures were analyzed based on the data reported by the authors (generally, without the use of atomic coordinates).

Table 3. X-ray diffraction data for large transition metal clusters

Composition	N^a	Packing^b	D^c/nm	$N_{BH}{}^d$	Reference	REFCODE
$[Pt_{19}(CO)_{22}]^{4-}(NBu_4^+)_4 \cdot 8MeCN$	19	I	0.6	2	41	BAPTCO
$[Os_{20}(CO)_{40}]^{2-}(PBu_4^+)_2$	20	f.c.c.	0.8	0	42	KINBUE10
$[Pd_{16}Ni_4(CO)_{22}(PPh_3)_4]^{2-}(PPh_4^+)_2 \cdot 2MeCN \cdot 1.64Me_2CO \cdot 0.64Pr_2O$	20	f.c.c.	0.8	0	43	QOSWOK
$[Os_{18}Hg_2(CO)_{42}C_2]^{4-}[C_{36}H_{30}NP_2]^+_4 \cdot CH_2Cl_2$	20*	O	1.2	0	44	VURXIP
$[Os_{18}Hg_2(CO)_{40}C_2]^{2-}[C_{36}H_{30}NP_2]^+_2$	20*	O	1.2	0	45	KICHEJ
$\{[Os_{10}(CO)_{24}Cl_2Hg\}^{2-}[C_{36}H_{30}NP_2]^+_2$	21*	O	1.4	0	46	SEKVEJ
$[Ag_{13}Fe_8(CO)_{32}]^{3-}[C_{36}H_{30}NP_2]^+_3 \cdot 2Me_2CO$	21	f.c.c.-Ag	0.9	1	47	ZATYIC
$[Ag_{13}Fe_8(CO)_{32}]^{4-}[C_{36}H_{30}NP_2]^+_4 \cdot 2Me_2CO$	21	f.c.c.-Ag	0.9	1	48	JUFGEW
$[Os_{18}Pd_3(CO)_{42}C_2][\{N(PPh_3)_2\}_2]$	21*	h.c.p.		0	49	
$Os_{12}Rh_9(CO)_{44}Cl \cdot 2(CH_2Cl_2)$	21	O	1.1	0	50	NIWYAT
$[Rh_{22}(CO)_{37}]^{4-}[C_9H_{22}N]^+_4$	22	ABCB	0.8	1	51	AMCORH
$[Pt_4Rh_{18}(CO)_{35}]^{4-}[C_8H_{20}N]^+_4 \cdot Me_2CO$	22	b.c.c.	0.9	2	52	SUBCAT
$[Rh_{22}(CO)_{35}H_n]^{5-n}[Cs_9(18\text{-}crown\text{-}6)_{14}]^{9+}$ ($n = 0, 1$)	22*	b.c.c.	0.9	2	53	ETCSRH
$[Rh_{23}(CO)_{38}N_4]^-[C_{24}H_{20}P]^+$	23*	A	0.9	2	54	KUMJIL
$Pd_{23}(CO)_{22}(PEt_3)_{10}$	23	f.c.c.	0.9	1	55	
$Pd_{23}(CO)_{20}(PEt_3)_8$	23	b.c.c.	0.9	1	56	
$[Ni_{14}Pt_{10}(CO)_{30}]^{4-}[NBu^n_4]^+_4 \cdot Me_2CO$	24	h.c.p.	0.9	2	57	NEPJUN
$[Pt_{24}(CO)_{30}]^{2-}L^+_2$ (L = PPh$_4$, AsPh$_4$, PMePh$_3$)	24	f.c.c.		1	58	
$[Ag_{12}Au_{12}NiCl_7(PPh_3)_{10}]^+[SbF_6]^- \cdot 15EtOH$	25	I	1.1	3	59	HEWSIL
$[Ag_{12}Au_{12}PtCl_7(PPh_3)_{10}]^+Cl^-$	25	I	1.1	3	60	YAWJOV
$Ag_{13}Au_{10}Pt_2Cl_7(PPh_3)_{10} \cdot 10Et_2O$	25	I	1.1	3	61	PINCEU
$Ag_{13}Au_{10}Pd_2Cl_7(PPh_3)_{10}$	25	I	1.1	3	62	
$Ag_{13}Au_{10}Ni_2Cl_7(PPh_3)_{10}$	25	I	1.1	3	62	
$\{Ag_{12}Au_{13}Cl_7[P(p\text{-}tol)_3]_{10}\}^{2+}[SbF_6]^-_2 \cdot xEtOH$	25	I	1.1	3	63	SOLCOL
$[Ag_{12}Au_{13}Cl_8(PMe_3)_{10}]^+[SbF_6]^-$	25	I	1.1	3	64	PIKNUS
$\{Ag_{12}Au_{13}Cl_8[P(p\text{-}tol)_3]_{10}\}^+[PF_6]^-$	25	I	1.1	3	65	
$[Ag_{12}Au_{13}Br_8(PPh_3)_{10}]^+Br^-$	25	I	1.1	3	66	YAWJUB
$\{Ag_{12}Au_{13}Br_8[P(p\text{-}tol)_3]_{10}\}^+[PF_6]^- \cdot 10EtOH$	25	I	1.1	3	67	SIBMUL
$[Ag_{12}Au_{13}Br_8(PPh_3)_{10}]^+[SbF_6]^- \cdot 20EtOH$	25	I	1.1	3	68	SOBWIP
$[Ag_{12}Au_{13}Br_8(PPh_3)_{10}]^+Br^- \cdot 3EtOH$	25	I	1.1	3	69	YAGKEW
$[Pt_{26}(CO)_{32}]^{2-}[PPh_3Me]^+_2$	26	h.c.p.		3	58	
$[Ru_{20}Cu_6(CO)_{48}H_4Cl_2]^{4-}[NBu_4]^+_4$	26*	O	1.6	0	70	PEBZIF
$[Pd_{13}Ni_{13}(CO)_{34}]^{4-}[PPh_4]^+_4$	26	ABCAC	0.9	1	71	
$[Rh_{28}(CO)_{41}H_2N_4]^{4-}[NEt_4]^+_4 \cdot Me_2CO$	28*	f.c.c.	0.9	3	72	TUCCID
$[Pd_{29}(CO)_{28}(PPh_3)_7]^{2-}[PPh_4]^+_2 \cdot 3MeCN$	29	f.c.c.	1.1	1	43	QOSXAX
$Pd_{30}(CO)_{26}(PEt_3)_{10} \cdot Me_2CO$	30	f.c.c.	1.1	2	73	
$[Pd_{16}Ni_{16}(CO)_{40}]^{4-}[NBu^n_4]^+_4$	32	ABCBCA		2	74	
$[Pd_{29}Ni_3(CO)_{22}(PMe_3)_{13}] \cdot 0.3(C_4H_8O)$	32	I	0.9	4	75	
$Pd_{34}(CO)_{24}(PEt_3)_{12}$	34	I		4	76	
$[HNi_{34}(CO)_{38}C_4]^{5-}[NMe_3CH_2Ph]^+_5$	34*	A		4	77	
$Pd_{35}(CO)_{23}(PMe_3)_{15} \cdot (C_4H_8O)$	35	I	1.0	5	75	
$[Ni_{31}Sb_4(CO)_{40}]^{6-}[NEt_4]^+_6 \cdot 2Me_2CO$	35	A	1.5	2	78	LOGLUO
$[Ni_{35}(CO)_{39}C_4]^{6-}[NEt_4]^+_6$	35*	A		4	77	
$[Ni_{30}Cu_5(CO)_{40}]^{5-}[NMe_4]^+_6Cl^- \cdot Me_2CO$	35	h.c.p.	1.0	3	79	QUDCEX
$Ag_{20}Au_{18}Cl_{14}(P(p\text{-}tol)_3)_{12}$	36	I	1.1	6	80	FUNFEZ
$Ag_{20}Au_{18}Cl_{14}(P(p\text{-}tol)_3)_{12} \cdot 42EtOH$	36	I	1.1	6	81	SIRRIU
$[Ag_{20}Au_{18}Cl_{12}(PPh_3)_{14}]^{2+}Cl^-_2 \cdot xEtOH$	36	I	1.1	6	82	HANFAD
$[Ag_{19}Au_{18}Br_{11}(P(p\text{-}tol)_3)_{12}]^{2+}[AsF_6]^-_2$	36	I	1.1	6	83	
$Pd_{38}(CO)_{28}(PEt_3)_{12} \cdot Me_2CO$	38	A	1.1	4	84	FIBBAT
$[Au_6Pd_6(Pd_{6-x}Ni_x)Ni_{20}(CO)_{44}]^{6-}[PPh_4]^+_6 \cdot 4.72MeCN \cdot Pr^i_2O$ ($x = 2.1-5.5$)	38	h.c.p.	1.1	6	85	
$[Au_6Ni_{32}(CO)_{44}]^{6-}[PPh_4]^+_6 \cdot 4.5MeCN$	38	h.c.p.	1.1	6	85	
$[Pt_{38}(CO)_{44}]^{2-}[AsPh_4]^+_2$	38	f.c.c.		6	58	
$[Ni_{24}Pt_{14}(CO)_{44}]^{4-}[NBu^n_4]^+_4 \cdot Me_2CO$	38	f.c.c.	0.9	6	57	NEPJOH
$[HNi_{38}(CO)_{42}C_6]^{5-}[N(C_4H_9)_4]^+_5$	38*	A		8	86	

Table 3 (*continued*)

Composition	N^a	Packing^b	D^c/nm	$N_{BH}{}^d$	Reference	REFCODE
$Pd_{39}(CO)_{23}(PMe_3)_{16}$	39	I	1.0	5	75	
$[Au_{39}Cl_6(PPh_3)_{14}]^{2+}Cl^-{}_2$	39	A	1.1	1	87	VUCSUH
$[Ag_{16}Ni_{24}(CO)_{40}]^{4-}[PPh_3Me]^+{}_4 \cdot Me_2CO \cdot 0.5(C_4H_8O)$	40	f.c.c.-Ag	1.0	4	88	
$[Au_{16}Ni_{24}(CO)_{40}]^{4-}[NMe_3Ph]^+{}_4$	40	f.c.c.-Au	1.0	4	89	
$[Ni_{36}Pt_4(CO)_{45}]^{6-}[NMe_3CH_2Ph]^+{}_6{}^e$	40	f.c.c.		4	90	
$[Ni_{37}Pt_4(CO)_{46}]^{6-}[NMe_3CH_2Ph]^+{}_6{}^e$	41	f.c.c.		4	90	
$Pd_{28}Pt_{13}(PPh_3)_{12}(PMe_3)H_{12}(CO)_{27} \cdot 5THF$	41*	h.c.p.	1.1	4	91	RUGCIF
$[Pd_{33}Ni_9(CO)_{41}(PPh_3)_6]^{4-}[C_{24}H_{20}P]^+{}_4 \cdot 5Me_2CO \cdot 3MeCN$	42	h.c.p.	1.2	1	92	TIXYAA
$[Ni_{38}Pt_6(CO)_{48}H_2]^{4-}[AsPh_4]^+{}_4$	44*	f.c.c.		6	93	
$[Ni_{38}Pt_6(CO)_{48}H]^{5-}[AsPh_4]^+{}_2[NBu_4]^+{}_3$	44*	f.c.c.		6	93	
$[Pt_{44}(CO)_{47}]^{4-}$	44	ABCBA		5	94	
$Ag_{45}(PPh)_{18}(PhPSiMe_3)_2Cl_7P(PPr^n{}_3)_{12}$	45*	S	1.9	1	95	RIDKEU
$[Pd_{20}Ni_{26}(CO)_{54}]^{6-}[NBu^n{}_4]^+{}_6$	46	f.c.c.			74	
$Ag_{50}(PPh)_{20}Cl_7P(PPr^n{}_3)_{13}$	50*	S		2	95	RIDKIY
$Pd_{54}(CO)_{40}(PEt_3)_{14}$	54	ABACA	1.5	6	73	
$Pd_{59}(CO)_{32}(PMe_3)_{21} \cdot 3Me_2CO \cdot 1.5Pr^i{}_2O$	59	A	1.3	11	75	
$Pd_{69}(CO)_{36}(PEt_3)_{18}$	69	I	1.4	15	96	
$Pd_{145}(CO)_{60}(PEt_3)_{30}$	145	I	1.7	55	97	LOVKIQ01

^{a} The total number of atoms in the metal polyhedron. Clusters containing interstitial metal atoms are marked with the sign *. Large clusters with nonmetal atoms inserted into the metal core are marked with an asterisk.
^{b} Packing modes: I is a local icosahedral or pentagonal-prismatic packing, f.c.c. is the face-centered cubic packing, h.c.p. is the hexagonal close packing (ABCB, *etc.* are arrangements of the layers in mixed f.c.c./h.c.p. packings), b.c.c. is the body-centered cubic packing, A is a distorted "amorphous" packing, S are shell clusters with a loose atomic packing, O are other packing modes.
^{c} The diameter of the metal core (the maximum interatomic distance).
^{d} The number of interstitial metal atoms, *i.e.*, metal atoms, which are located inside the cluster and are not coordinated by the ligands.
^{e} The full stoichiometric composition of the compound: $0.5\{[Ni_{36}Pt_4(CO)_{45}]^{6-}[NMe_3CH_2Ph]^+{}_6\} \cdot 0.5\{[Ni_{37}Pt_4(CO)_{46}]^{6-}[NMe_3CH_2Ph]^+{}_6\} \cdot C_3H_8O$.

structures of the ligand shells formed by light atoms were established only tentatively.

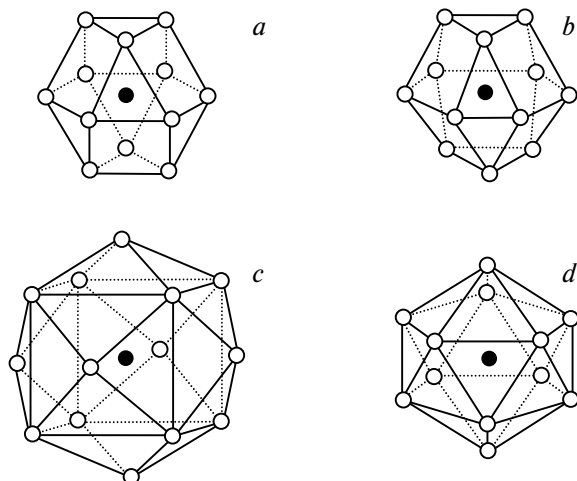The atomic packings in the clusters were related to the corresponding idealized types of atomic packing in crystalline metals: the face-centered cubic packing consisting of close-packed hexagonal layers ...ABCABC..., the hexagonal closest packing with the ...ABAB... arrangement of layers, other close packings of layers (for example, the mixed close packing ABCBA), and the body-centered cubic packing as well as the local icosahedral packing (I), which does not occur in an infinite crystal but can exist in finite-size clusters (see above). The geometry of the local environment of the atoms in these packings is shown in Fig. 4. In addition, Table 3 gives examples of strongly distorted "amorphous" (A) and "shell" (S) clusters, which are not described by a particular idealized packing mode. The structures of all these clusters are discussed in the next section.

Fig. 4. Types and symmetry of the local environment in close atomic packings: (*a*) cuboctahedron (f.c.c., O_h); (*b*) twinned cuboctahedron (h.c.p., D_{3h}); (*c*) hexacapped cube or tetrahexahedron (b.c.c., O_h); (*d*) centered icosahedron (icosahedral local packing, I_h).

3. Types of atomic packing in large clusters based on X-ray diffraction data

3.1. Face-centered cubic packing

The face-centered cubic close packing is typical of many metals. Each atom in this packing is surrounded by 12 nearest atoms to form a cuboctahedron (see Fig. 4, *a*). Some clusters containing high-symmetry metal cores corresponding to the f.c.c. packing are shown in Fig. 5.
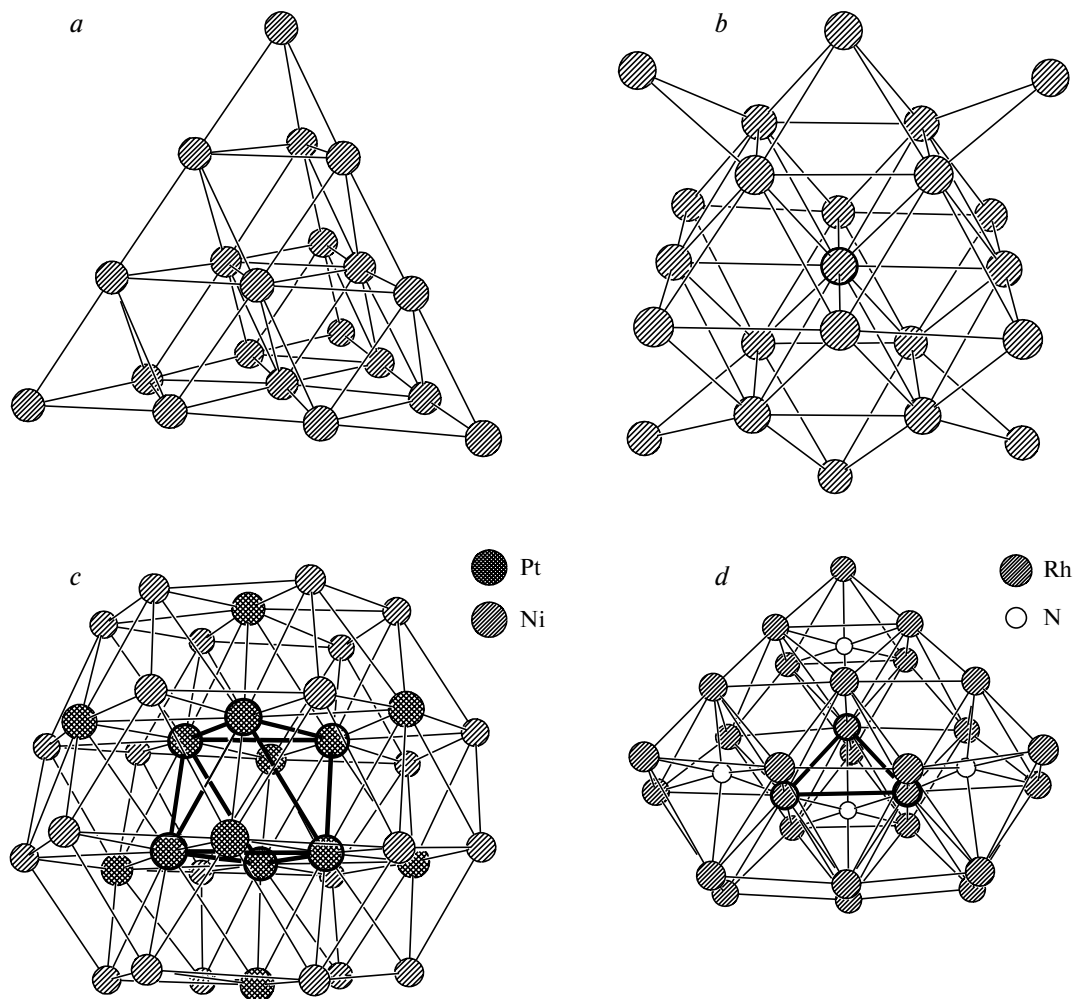
Fig. 5. Metal cores with the f.c.c. packing (interstitial atoms are marked): (a) $[Os_{20}(CO)_{40}]^{2-}$,[42] (b) $Pd_{23}(CO)_{22}(PEt_3)_{10}$,[55] (c) $Ni_{24}Pt_{14}(CO)_{44}]^{4-}$,[57] and (d) $[Rh_{28}(CO)_{41}H_2N_4]^{4-}$.[72]

The $[Os_{20}(CO)_{40}]^{2-}$ [42] cluster anion (see Fig. 5, *a*) can serve as one of the most simple and illustrative examples of a fragment of the f.c.c. packing. The v_3-tetrahedral cluster core is composed of triangular layers consisting of three, six, and ten Os atoms located below one atom (vertex of the polyhedron) according to the ABCA motif. Analogously, the v_3 tetrahedron Os_{20} can be divided into layers (1:3:6:10) with respect to any of its four vertices. In the first coordination sphere, the Os—Os distances are in the range of 2.67—2.81 Å; the average value (2.76 Å) is somewhat larger than the shortest interatomic distance (2.68 Å) in h.c.p. bulk osmium metal (see Table 1). All carbonyl ligands in this cluster are terminal. The Os atoms at the vertices of the tetrahedron, on the edges of the tetrahedron, and at the centers of its faces are coordinated by three CO ligands, two CO ligands, and one CO ligand, respectively. It should be noted that the metal core of this cluster contains no interstitial atoms; the maximum coordination number of the Os atoms in the cluster (for the Os atoms in the centers of

the v_3-triangular faces) is 9. The metal core of the $[Pd_{16}Ni_4(CO)_{22}(PPh_3)_4]^{2-}$ cluster[43] in which the Ni atoms are located at the vertices of the v_3 tetrahedron has an analogous structure.

The structure of the $Pd_{23}(CO)_{22}(PEt_3)_{10}$ cluster[55] is shown in Fig. 5, *b*. There is one Pd atom inside the cluster metal core. The nearest environment of this Pd atom is a cuboctahedron formed by 12 palladium atoms located at distances of 2.70—2.91 Å. Six square faces of the cuboctahedron are capped with the $PdPEt_3$ vertices giving rise to the v_2 octahedron Pd_{19} in which four triangular faces are additionally capped with the exopolyhedral μ_2-$Pd(CO)_2PEt_3$ fragments. The average shortest Pd—Pd distance between the central and peripheral atoms (2.85 Å) is almost equal to the average periphery—periphery distance in the v_2 octahedron Pd_{19}, and these distances are also longer than the shortest interatomic distance in palladium metal (2.75 Å), whereas the Pd—Pd bonds involving the exopolyhedral atoms linked through the μ_2-CO ligands are shortened to 2.73 Å (aver.). The metal core

Pd_{23} has the idealized D_{2h} symmetry and is coordinated also by the μ_2- and μ_3-bridging CO groups.

The 38-atom metal core of the $[Ni_{24}Pt_{14}(CO)_{44}]^{4-}$ cluster[57] (see Fig. 5, *c*) is the ν_3 octahedron without vertices (see Fig. 3, *b*). Four layers (7:12:12:7 atoms) form a fragment of the f.c.c. packing. Each seven-atom layer is a hexagon consisting of Ni atoms and centered with the Pt atom. Each 12-atom layer is the ν_4 triangle Ni_6Pt_6 without vertices in which the Pt atoms form the inner ν_2 triangle. Six interstitial Pt atoms form an octahedron. All faces of the latter are capped with the exopolyhedral Pt atoms bound to the Ni atoms and CO ligands. Therefore, each interstitial Pt atom has a cuboctahedral environment formed by eight Pt atoms (2.73—2.88 Å) and four Ni atoms (2.58—2.66 Å). The average shortest Pt—Pt distance (2.77 Å) is equal to the interatomic distance in bulk platinum metal, whereas the average Pt—Ni and Ni—Ni distances (2.66 and 2.66 Å, respectively) differ substantially from the sums of the corresponding atomic radii, which is indicative of strong strains in the metal core (see Table 1). The ligand shell of the cluster consists of 26 terminal and 18 μ_2-bridging CO ligands. In the homoatomic $[Pt_{38}(CO)_{44}]^{2-}$ cluster, the metal core with the O_h symmetry has an analogous structure. In this cluster, the carbonyl ligands have not been revealed from X-ray diffraction data.[58]

Two isostructural clusters of the general formula $[Ni_{38}Pt_6(CO)_{48}H_{6-n}]^{n-}$ (*n* = 4 or 5),[93] which are geometrically related to the above-considered 38-atom clusters, contain a 44-atom core with a two-shell octahedral (O_h) structure. An octahedron consisting of six Pt atoms is located inside the ν_3-octahedral metal shell Ni_{38} (see Fig. 3, *c*). The closest environment of each Pt atom, like that in $Ni_{24}Pt_{14}$, is a cuboctahedron formed by four Pt atoms and eight Ni atoms. A comparison of the average metal—metal distances (Pt—Pt, 2.72 Å; Pt—Ni, 2.63 Å; and Ni—Ni, 2.58 Å) with the shortest interatomic distances in platinum metal (2.78 Å) and nickel metal (2.49 Å) shows that the interstitial Pt atoms are substantially "contracted," whereas the radii of the exopolyhedral Ni atoms increase.

The metal core of the $[Rh_{28}(CO)_{41}H_2N_4]^{4-}$ cluster[72] (see Fig. 5, *d*) consists of four layers formed by Rh atoms (7:10:7:4). This cluster contains three interstitial Rh atoms, which have a cuboctahedral nearest environment. The average shortest Rh—Rh distances are 2.75, 2.93, and 2.87 Å in the inner triangle, between the exopolyhedral and interstitial atoms, and between two exopolyhedral atoms, respectively (as opposed to 2.69 Å in metal, see Table 1). The exopolyhedral Rh atoms are coordinated by 15 terminal and 26 μ_2-bridging carbonyl ligands as well as by two μ_2-H ligands. The octahedral cavities in the cluster core are occupied by four interstitial μ_6-N atoms. The edges in the octahedral cavities containing the N atoms are somewhat elongated (2.74—3.27 Å,

aver. 2.90 Å) compared to the remaining portion of the cluster (2.58—3.08 Å, aver. 2.87 Å).

The $[Pd_{29}(CO)_{28}(PPh_3)_7]^{2-}$ cluster anion[43] containing one interstitial Pd atom is built from three layers (3:10:15), which are ν_1, ν_3, and ν_4 triangles, respectively, to form the f.c.c. packing. This three-layer 28-atom core has one interstitial Pd atom; yet another Pd atom is located above the "upper" Pd_3 triangle. The Pd—Pd distances involving the interstitial atoms are in the range of 2.75—2.83 Å. The Pd—Pd distances between the exopolyhedral atoms are in the range of 2.69—3.21 Å. The average distances (2.79 and 2.82 Å, respectively) are somewhat larger than twice the metallic radius of Pd (see Table 1). The cluster core is coordinated by 15 μ_2-bridging and 13 μ_3-bridging CO ligands.

The core of the cluster f.c.c. $[Pt_{24}(CO)_{30}]^{2-}$ anion[58] has the idealized C_{2v} symmetry and is composed of three close-packed hexagonal layers (5:9:10). The first layer, which consists of five Pt atoms and can be described as a ν_2 triangle without one vertex, is closely stacked onto a ν_3 triangle without one vertex. The third layer consisting of ten Pt atoms is a fragment of a ν_4 triangle. The cluster contains one interstitial Pt atom in the cuboctahedral nearest environment. The metal core is coordinated by 22 terminal and eight μ_2-bridging CO ligands.

The cluster core of $Pd_{30}(CO)_{26}(PEt_3)_{10}$ [73] consists of four layers (6:7:7:6), which form a fragment of the f.c.c. packing. The six-atom layers can be described as ν_2 triangles. The layers consisting of seven atoms are centered hexagons. Two μ_2- and two μ_3-Pd caps are attached to the f.c.c. Pd_{26} fragment. The cluster has two interstitial metal atoms.

The histograms of the metal—metal interatomic distances in some f.c.c.-type metal cores are shown in Fig. 6. The positions of the maxima of RDF in these histograms are consistent with the idealized f.c.c.-packed coordination spheres, which are shown by dashes at the top of the histograms. The relative heights of these maxima and their average coordination numbers depend on the size and shape of the polyhedron. The high-symmetry ν_3 tetrahedron Os_{20} (see Fig. 5, *a*) has narrow maxima of the coordination spheres (see Fig. 6, *a*), whereas the centered ν_2 octahedron Pd_{19} capped with four asymmetrical fragments displays a broadening of the maxima (see Fig. 6, *b*). A further smearing of the coordination spheres is observed in the heterometallic $Ni_{24}Pt_{14}$ core (see Fig. 6, *c*) and the $Rh_{28}H_2N_4$ cluster containing the hydride and nitride atoms in the cavities of the packing (see Fig. 6, *d*). In the latter two clusters, the adjacent spheres overlap at distances $R > 5—6$ Å, which hinders the unambiguous assignment of the packing mode based on the histogram. Therefore, one-dimensional radial distribution functions allow one to characterize the atomic packings in an undistorted metal core, but provide much less information on the structures of distorted clusters.
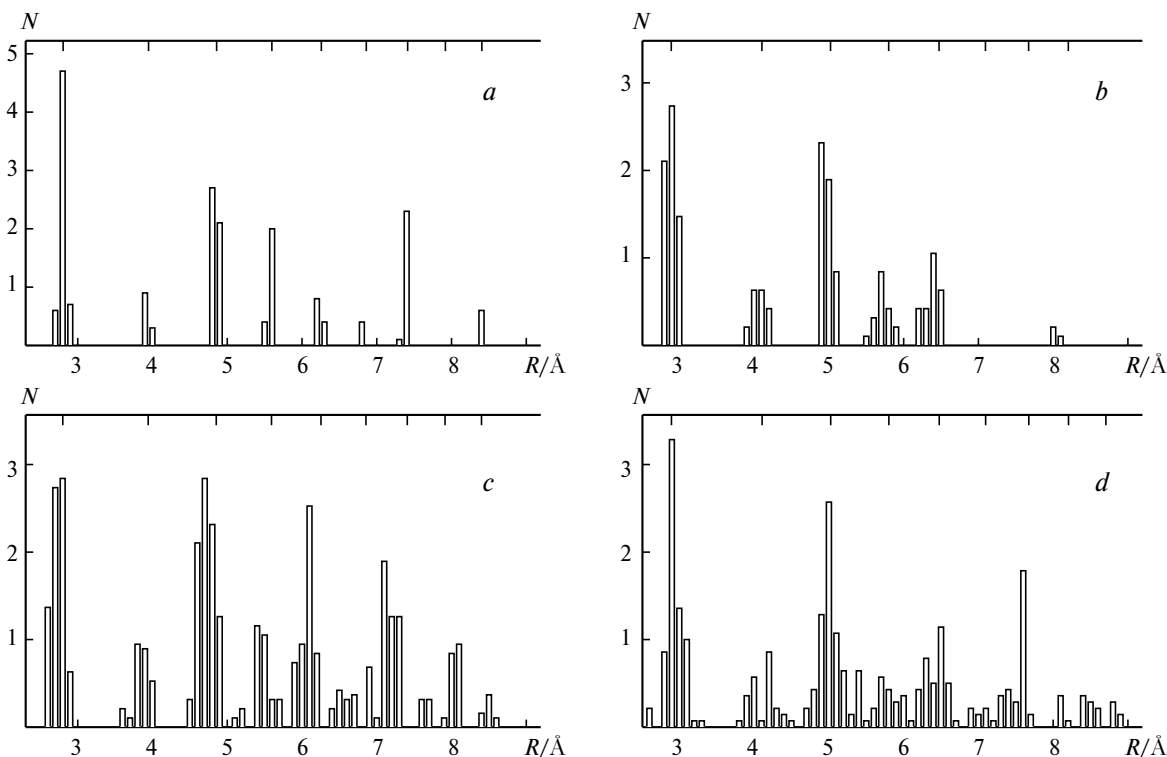
Fig. 6. Histograms of the M—M interatomic distances in the metal cores of the f.c.c. type: (*a*) $[Os_{20}(CO)_{40}]^{2-}$,[42] (*b*) $Pd_{23}(CO)_{22}(PEt_3)_{10}$,[55] (*c*) $Ni_{24}Pt_{14}(CO)_{44}]^{4-}$,[57] and (*d*) $[Rh_{28}(CO)_{41}H_2N_4]^{4-}$.[72] The coordination spheres in the ideal f.c.c. packing normalized to the average distance $R = a$ in the first coordination sphere (see Table 2) are indicated by dashes at the top of the plot.

Of compounds listed in Table 3, the bimetallic clusters $[Ag_{13}Fe_8(CO)_{32}]^{3-}$,[47] $[Ag_{13}Fe_8(CO)_{32}]^{4-}$,[48] $[Ag_{16}Ni_{24}(CO)_{40}]^{4-}$,[88] and $[Au_{16}Ni_{24}(CO)_{40}]^{4-}$[89] are also characterized by f.c.c.-type packings of the Ag and Au atoms. The same packing is observed in the $[Ni_{36}Pt_4(CO)_{45}]^{6-}$[90] and $[Ni_{37}Pt_4(CO)_{46}]^{6-}$ clusters[90] containing an inner tetrahedron of Pt atoms. For a series of 55-atom clusters, which do not form single crystals (such as $Au_{55}(PPh_3)_{12}Cl_6$,[98] $Rh_{55}(PBu^t_3)_{12}Cl_{20}$,[99] $Ru_{55}(PBu^t_3)_{12}Cl_{20}$, $Rh_{55}(PPh_3)_{12}Cl_6$, and $Pt_{55}(AsBu^t_3)_{12}Cl_{20}$[100]), the f.c.c. packing was revealed by indirect structural methods, including high-resolution transmission electron microscopy (HRTEM). The cluster cores in these compounds consist, presumably, of the centered 13-atom cuboctahedron surrounded by the 42-atom shell (Chini's magic numbers $10k^2 + 2$ of atoms for $k = 1$ and 2, see Section 2).

3.2. Hexagonal close packing

In the hexagonal close packing (h.c.p.) with the ...ABABA... arrangement of the close-packed hexagonal layers, each atom is surrounded by 12 neighbors to form a twinned cuboctahedron (see Fig. 4, *b*). Among medium-sized clusters, the $[Ni_{12}(CO)_{21}H_{4-n}]^{n-}$ ($n = 2$—4)[101] and $[Rh_{13}(CO)_{24}H_{5-n}]^{n-}$ anions ($n = 2$—4)[24] represent frag-

ments of h.c.p. Examples of selected large h.c.p. polyhedra are presented in Fig. 7.

In the $[Os_{18}Pd_3(CO)_{42}C_2]^{2-}$ cluster anion,[49] the metal core with the idealized D_{3h} symmetry can be considered as a fragment of h.c.p. consisting of five layers (6:3:3:3:6, ABABA arrangement); the central layer is formed by Pd atoms, whereas the outer layers are v_2 triangles formed by Os atoms. This cluster contains no interstitial metal atoms.

The core of the $[Pt_{26}(CO)_{32}]^{2-}$ cluster anion[58] is a fragment of h.c.p. formed by Pt atoms with the idealized D_{3h} symmetry and consists of three hexagonal layers (7:12:7) arranged according to the ABA motif. The layers consisting of seven Pt atoms are centered hexagons, whereas the 12-atom layer can be described as a v_4 triangle without vertices. The Pt_{26} metal core containing three interstitial metal atoms is coordinated by 23 terminal and nine μ_2-bridging CO ligands.

The metal polyhedron of the $[Ni_{14}Pt_{10}(CO)_{30}]^{4-}$ cluster[57] (see Fig. 7, *a*) consists of three layers (7:10:7) characterized by the h.c.p.-type arrangement. The distance between two interstitial Pt atoms is 2.63 Å, each Pt atom being in a twinned cuboctahedral environment formed by six Pt atoms (Pt—Pt, 2.61—2.82 Å; aver. 2.73 Å), three Ni atoms (Pt—Ni, 2.70—2.85 Å; aver. 2.75 Å), and three disordered Pt/Ni positions, because two of ten Pt atoms
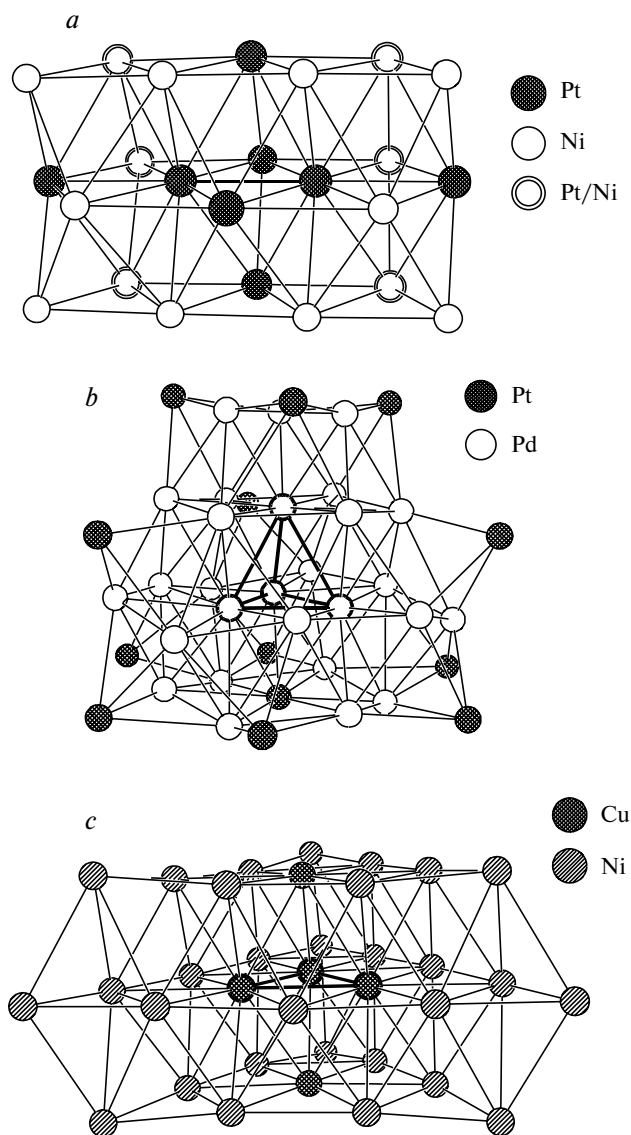
Fig. 7. Metal cores with h.c.p.-type close packings (interstitial fragments are shown): (*a*) $[Ni_{14}Pt_{10}(CO)_{30}]^{4-}$,[57] (*b*) $Pd_{28}Pt_{13}(PPh_3)_{12}(PMe_3)H_{12}(CO)_{27}$,[91] and (*c*) $[Ni_{30}Cu_5(CO)_{40}]^{5-}$.[79]

are disordered over six positions in the metal polyhedron with partial occupancies.

Yet another example of the bimetallic h.c.p. clusters is $Pd_{28}Pt_{13}(PPh_3)_{12}(PMe_3)H_{12}(CO)_{27}$[91] (see Fig. 7, *b*). Its metal core consists of the $Pd_{28}Pt$ moiety, whose square faces are capped with Pt atoms, which do not form short contacts with each other. The distorted 38-atom fragment of h.c.p. includes four layers (6:7:12:13) and is additionally capped with three Pt atoms. The first layer consisting of six metal atoms (the upper layer in Fig. 7, *c*) can be described as a v_2 triangle consisting of three Pd atoms (which form an inner v_1 triangle) and three Pt atoms at the vertices. The second layer consists of seven Pd atoms

that form a centered hexagon. The third layer is composed of 12 Pd atoms that form a v_4 triangle without vertices. In the fourth layer consisting of 13 atoms, the central Pt atom is in the planar hexagonal environment formed by Pd atoms, and six more Pd atoms are bound to each edge of the hexagon. The metal core has the idealized C_3 symmetry axis perpendicular to the atomic layers. The cluster contains four interstitial Pd atoms, which form a tetrahedron with edge lengths varying in the range of 2.65—2.82 Å (average length is 2.73 Å; this value is somewhat smaller than the shortest interatomic distance in the bulk metal). The binding interatomic distances involving the interstitial Pd atoms are in the ranges of 2.65—3.09 Å (Pd—Pd) and 2.81—2.83 Å (Pd—Pt), their average values being equal (2.82 Å). In the overall cluster, the distances between the adjacent atoms are in the ranges of 2.65—3.20 Å (Pd—Pd, aver. 2.83 Å) and 2.64—3.25 Å (Pd—Pt, aver. 2.84 Å), which are indicative of a weakening of the metal—metal interactions. The fact that the Pt—Pt distances are close to the Pt—Pd distances reflects the similarity of their atomic radii due to lanthanide contraction. An elongation of the M—M bonds by 0.05—0.10 Å compared to those in the bulk metals is observed in a series of f.c.c. and h.c.p. clusters with a carbonyl ligand environment.

The $[Ni_{30}Cu_5(CO)_{40}]^{5-}$ cluster anion[79] (see Fig. 7, *c*) with the idealized D_{3h} symmetry consists of three layers (10:15:10; ABA motif), which can be described as two v_3 triangles Ni_9Cu and one inner v_4 triangle $Ni_{12}Cu_3$. The Cu atoms located at the centers of the triangular layers form a trigonal bipyramid with the shortest Cu—Cu distances in the range of 2.41—2.52 Å. The average Cu—Cu distance (2.46 Å) is shorter than the shortest interatomic distance in bulk copper (2.56 Å), whereas the average binding Ni—Ni distance (2.53 Å) in this cluster is slightly longer than the corresponding distance in bulk nickel (2.49 Å, see Table 1). The cluster contains three interstitial Cu atoms in a twinned cuboctahedral environment formed by eight Ni atoms (2.46—2.60 Å) and four Cu atoms (2.41—2.52 Å). The metal core is coordinated by seven μ_3-bridging and 24 μ_2-bridging CO ligands as well as by nine terminal CO ligands.

The $[Pd_{33}Ni_9(CO)_{41}(PPh_3)_6]^{4-}$ anion[92] (Fig. 8, *a*) also belongs to the group of clusters, whose idealized metal core reproduces a fragment of h.c.p. The core of this bimetallic 42-nuclear cluster consists of five layers (10:6:10:6:10), which can be described as v_3 and v_2 triangles stacked to form the ABABA motif. The vertices of the v_3 triangles are occupied by the Ni atoms. The metal atoms on the surface of the polyhedron are coordinated by carbonyl ligands. The Ni atoms in two outer v_3 triangles are coordinated also by the phosphine ligands. The idealized point symmetry group of the cluster is D_{3h}. In spite of the large number of atoms, the metal core has only one interstitial Pd atom in a twinned cuboctahedral
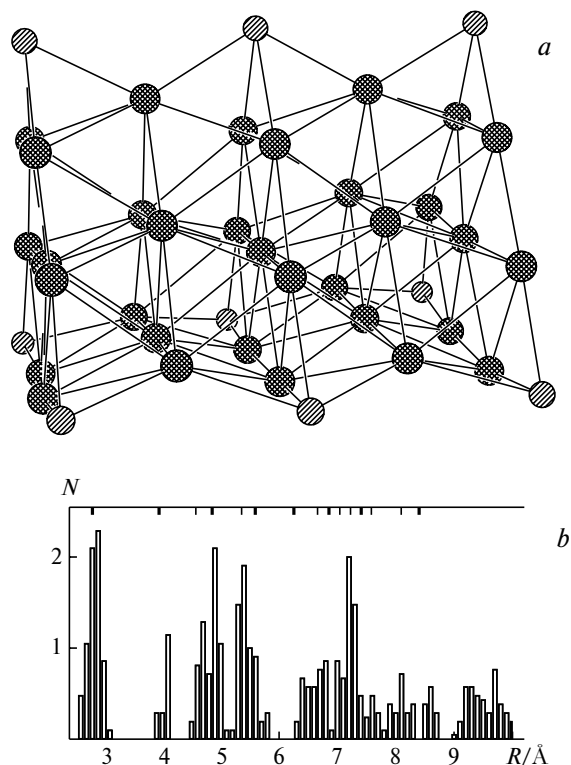
Fig. 8. Metal core (*a*) and a histogram of the M—M interatomic distances (*b*) in the h.c.p. $[Pd_{33}Ni_9(CO)_{41}(PPh_3)_6]^{4-}$ cluster.[92] The coordination spheres specific for h.c.p. are indicated by thin dashes; the coordination spheres common to h.c.p. and f.c.c. are shown by bold dashes (normalized to the average distance $R = a$ in the first coordination sphere) at the top of the plot.

environment formed by 12 Pd atoms at distances of 2.78—2.82 Å. The Pd—Pd bond lengths in the cluster core are in the range of 2.69—3.03 Å (average length (2.83 Å) is somewhat larger than the distance (2.75 Å) in the bulk metal). The Pd—Ni bond lengths are in the range of 2.55—2.71 Å (average length (2.63 Å) is virtually equal to the sum of the metallic radii). Therefore, no essential contraction of the atoms is observed in this h.c.p. cluster as well.

The atomic environment in the ideal hexagonal close packing contains spheres characteristic of f.c.c. and closely spaced neighboring spheres specific for h.c.p. (see Table 1). Since the spheres separated by distances of 0.2—0.3 Å are generally not resolved in the structures of real clusters, one-dimensional histograms of interatomic distances in the h.c.p. are similar to those in the distorted f.c.c packing.* In the bimetallic h.c.p. clusters containing atoms with substantially different radii, the maxima of the coordination spheres are additionally broadened. The radial distribution histogram for the above-described h.c.p.-type $Pd_{33}Ni_9$ metal core is shown in Fig. 8, *b*. In

_____
* Two-dimensional polar diagrams proposed in the study[35] allow one to distinguish between f.c.c. and h.c.p. clusters.

this rather rare case, the h.c.p. closest coordination spheres can be identified along with the f.c.c.-type spheres; however, the maxima of RDF at distances larger than 6 Å are broadened and smeared. In most of the structurally studied h.c.p. clusters, it is difficult to determine the packing of metal atoms based on one-dimensional RDF without recourse to supplementary data.

According to the results of X-ray diffraction analysis, a fragment of h.c.p. is also present in the isostructural 38-nuclear $[Au_6Ni_{32}(CO)_{44}]^{6-}$ and $[Au_6Pd_6(Pd_{6-x}Ni_x)Ni_{20}(CO)_{44}]^{6-}$ cluster anions ($x = 2.1—5.5$)[85] containing a four-layer 30-atom core (3:12:12:3; the ABAB arrangement of layers perpendicular to the non-crystallographic C_3 axis with the "upper" and "lower" Ni caps). The resulting 32-atom fragment of h.c.p. is capped with six Ni atoms to form a metal polyhedron with the idealized D_{3d} symmetry. In the trimetallic clusters, the Pd atoms occupy the upper and lower v_1-triangular layers (average Pd—Pd distance is 2.92 Å) and the disordered positions in the central 12-atom layers, which can be described as v_4 triangles without vertices. Six interstitial gold atoms in three structurally studied clusters of this type form an octahedron in which the average distances (2.84—2.86 Å) are close to the shortest Au—Au distance in bulk gold (2.88 Å). The Ni—Ni distances in the layers are substantially elongated (aver. 2.59 Å), whereas the distances between the layers are shortened (aver. 2.42 Å). The metal core is coordinated by eight terminal, 30 μ_2-bridging, and four μ_3-bridging CO ligands.

3.3. Other combinations of close-packed hexagonal layers

In large transition metal clusters, other types of close packing with a mixed motif of close-packed hexagonal atomic layers can also occur. For example, the $[Rh_{22}(CO)_{37}]^{4-}$ cluster anion[51] (Fig. 9, *a*) belongs to structures, whose idealized metal core contains fragments of both f.c.c. and h.c.p. The core of this cluster with the C_{3v} point symmetry consists of four layers (3:6:7:6) (normal triangle, a v_2 triangle, a centered hexagon, and one more v_2 triangle, respectively) stacked in the ABCB order. The cluster has one interstitial Rh atom (in layer "C") in a twinned cuboctahedral environment formed by 12 Rh atoms at essentially elongated distances (2.76—2.83 Å; aver. 2.80 Å, see Table 1). In the entire cluster, the Rh—Rh bond lengths are in the range of 2.73—2.88 Å. The metal core is coordinated by the bridging and terminal CO ligands. The ABCB packing of the layers in the infinite crystal lattice was found in several rare-earth metals (La, Nd, Pr).[102]

The $[Pt_{44}(CO)_{47}]^{4-}$ cluster[94] contains a fragment of the ABCBA packing. Its metal core with the D_{3h} symmetry consists of five layers (6:10:12:10:6), which can be described as a v_2 triangle, a v_3 triangle, a v_4 triangle without three vertices, a v_3 triangle, and a v_2 triangle, respec-
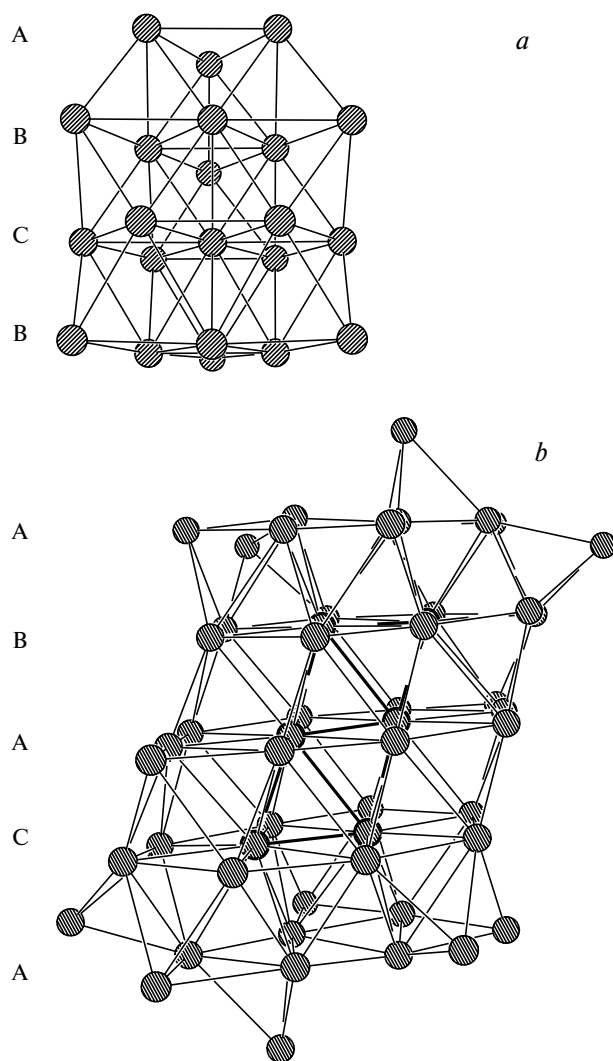
Fig. 9. Metal cores with a mixed f.c.c./h.c.p. packing: (*a*) $[Rh_{22}(CO)_{37}]^{4-}$ [51] (ABCB) and (*b*) $Pd_{54}(CO)_{40}(PEt_3)_{14}$ (ABACA).[73] The motifs of stacking of the layers are denoted; in $Pd_{54}(CO)_{40}(PEt_3)_{14}$, the six-atom inner fragment is marked off.

tively. The cluster has five interstitial Pt atoms, which form a trigonal bipyramid.

The metal core of the $[Pd_{13}Ni_{13}(CO)_{34}]^{4-}$ cluster anion[71] with the idealized C_{3v} symmetry is a fragment of the ABCAC packing. The first four layers, *viz.*, ABCA (1:3:6:10), can be described as a 20-atom ν_3 tetrahedron analogous to the f.c.c. $[Os_{20}(CO)_{40}]^{2-}$ [42] and $[Pd_{16}Ni_4(CO)_{22}(PPh_3)_4]^{2-}$ clusters.[43] The Ni_3 triangle, the ν_2 triangle consisting of six Pd atoms, and the ν_3 triangle Pd_7Ni_3 with the Ni atoms at the vertices are located under the "upper" Ni atom. The positions of the atoms in the fifth Pd_3Ni_3 layer (ν_2 triangle with the Ni atoms at the vertices), which violates the f.c.c. packing, are located under the atoms of the third layer. The cluster contains one interstitial Pd atom in the closest twinned cuboctahedral environment.

In the $[Pd_{16}Ni_{16}(CO)_{40}]^{4-}$ cluster,[74] the metal atoms form the six-layer closest packing ABCBCA (3:6:7:7:6:3). The layers are the Ni_3 triangles, the ν_2 triangles Ni_3Pd_3 with the Ni atoms at the vertices, and the centered hexagons Pd_5Ni_2. The cluster contains two interstitial Pd atoms in a twinned cuboctahedral environment formed by ten Pd atoms and two Ni atoms.

The $Pd_{54}(CO)_{40}(PEt_3)_{14}$ cluster[73] (see Fig. 9, *b*) consists of five layers (8:10:12:10:8), which form the ABACA-type closest packing. Each ten-atom layer contains two interstitial Pd atoms in a twinned cuboctahedral environment, whereas two interstitial atoms of the central 12-atom layer have a cuboctahedral environment. Therefore, 48 Pd atoms form the ABACA core containing a planar six-atom interstitial fragment, which is additionally coordinated by six μ_3-Pd caps. The Pd—Pd distances between the interstitial atoms (2.70—2.81 Å; aver. 2.76 Å) are similar to those in the bulk metal. The remaining distances are as follows: Pd_{inter}—Pd_{exopol} are 2.72—3.00 Å and Pd_{exopol}—Pd_{exopol} are 2.65—3.12 Å.

Generally, an overlapping and coalescence of closely spaced spheres in the radial distribution histograms, which are mentioned above for the h.c.p.-type metal cores, do not allow one to reveal a mixed packing based solely on the "one-dimensional" data. In some cases (see Fig. 9, *a*, the Rh_{22} core), the closest h.c.p.- and f.c.c.-type metal—metal spheres are split; however, in most cases, they coalesce to form a broad sphere (see Fig. 9, *b*, Pd_{54} core). Diffuse maxima of the coordination spheres are indicative of distortions of the metal core. However, the average interatomic distances in the above-considered homometallic clusters provide evidence that distortions of the f.c.c. and h.c.p. packings in these clusters are not accompanied by substantial deformations of the atomic radii. The common feature of the RDF of all such clusters (f.c.c., h.c.p., and mixed packings) is the presence of a pronounced "second" maximum at $\sim a\sqrt{2}$, where a is the interatomic distance in the first metal—metal coordination sphere.

3.4. Body-centered cubic packing

In the body-centered cubic (b.c.c.) packing, each atom is surrounded by 14 neighbors (see Fig. 4, *c*). Eight neighboring atoms are located at the shortest distance a to form a cube. In the ideal b.c.c. packing, the distance between the central atoms and the remaining six atoms located above the square faces of the cube at the vertices of the octahedron is $\sqrt{(4/3)}a = 1.1547a$. Among medium-sized clusters, the 14-nuclear $[Rh_{14}(CO)_{25}]^{4-}$ anion corresponds to a distorted b.c.c. packing.[103]

The $[Pt_4Rh_{18}(CO)_{35}]^{4-}$ cluster[52] (Fig. 10, *a*) serves as an example of large b.c.c.-type metal cores. Four Pt atoms form a tetrahedron, whose two vertices are occupied by interstitial atoms. The distances between the interstitial Pt atoms (2.56 Å) are shorter than the remaining Pt—Pt
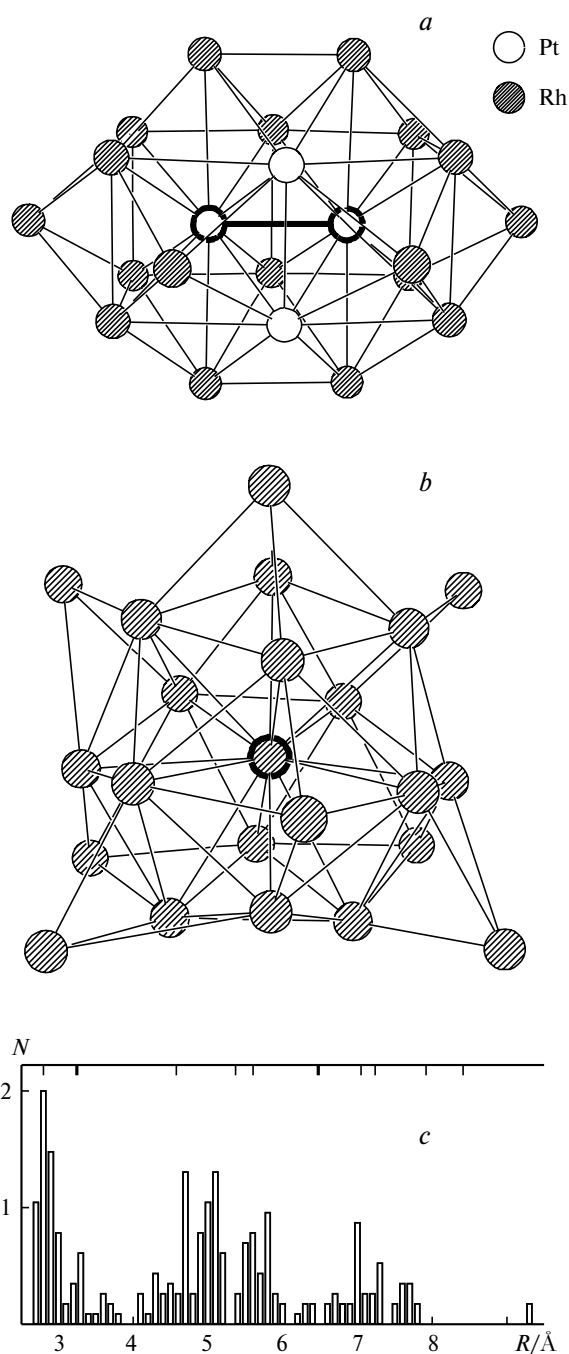
Fig. 10. Metal cores with a b.c.c. packing: (*a*) $[Pt_4Rh_{18}(CO)_{35}]^{4-}$ [52] and (*b*) $Pd_{23}(CO)_{20}(PEt_3)_8$ [56] (interstitial atoms are marked off); (*c*) histogram of the Pd—Pd interatomic distances in $Pd_{23}(CO)_{20}(PEt_3)_8$. The coordination sphere specific for b.c.c. are indicated by bold dashes at the top of the plot (*c*); the coordination spheres, which are present also in f.c.c. and/or h.c.p. packings, are shown by thin dashes.

distances (2.69—2.83 Å). Each interstitial Pt atom is surrounded by 13 neighbors, including a cube formed by six Rh atoms (2.66—2.79 Å) and two Pt atoms (2.69—2.71 Å) as well as an incomplete octahedron consisting of four Rh

atoms (3.07, 3.15, 3.35, and 3.51 Å) and one interstitial Pt atom (2.56 Å). Therefore, two interstitial Pt atoms are located inside the double cube formed by ten Rh atoms and two Pt atoms. The square faces of this polyhedron are capped with eight Rh atoms. However, the two opposite Rh—Rh bonds between the vertices shared by two cubes are absent (distances are 3.88—3.93 Å) in this double cube, in contrast to the idealized b.c.c. packing. This elongation along with a shortening of the Pt—Pt distance in the polyhedron by 0.2 Å compared to that observed in the bulk metal are indicative of strong strains within the metal polyhedron. The metal core is coordinated by the terminal and bridging carbonyl ligands.

The metal cores of the $[Rh_{22}(CO)_{35}H_n]^{5-n}$ clusters ($n = 0, 1$) [53] have similar structures. The distance between two interstitial Rh atoms (2.492 Å), which are surrounded by 13 Rh atoms each, is shorter than that in the f.c.c. rhodium metal (2.630 Å; see Table 1). The interstitial atoms are located inside the double cube formed by 12 Rh atoms. The square faces of this cube are coordinated by eight Rh caps. As in the above-described cluster, two opposite Rh—Rh bonds shared by two "fused" cubes are absent.

The metal polyhedron of the $Pd_{23}(CO)_{20}(PEt_3)_8$ cluster [56] (see Fig. 10, *b*) can also be assigned to a strongly distorted fragment of a b.c.c.-type packing. The cluster has one interstitial Pd atom bound to 14 neighbors at distances of 2.81—3.02 Å (aver. 2.92 Å). The environment of the central atom resembles a distorted fragment of a b.c.c.-type packing. However, the Pd—Pd bond lengths involving the central atom are equalized, which corresponds to an elongation of the Pd—Pd bonds within the first coordination sphere and a shortening of the Pd—Pd bonds within the second closest coordination sphere. An increase in the coordination number of the interstitial Pd atom to 14 is accompanied by a substantial increase in the average binding metal—metal distance. Distortions in the nearest environment about the central atom lead to cleavage of four Pd—Pd bonds between the vertices of the cube, which should occur in the idealized b.c.c. packing (corresponding distances are larger than 4 Å). The 15-atom distorted fragment of b.c.c. is coordinated by eight PdPEt_3 caps and 20 bridging carbonyl ligands.

The difference in the packing of the Pd atoms in the $Pd_{23}(CO)_{22}(PEt_3)_{10}$ (f.c.c., see Figs. 5, *b* and 6, *b*) and $Pd_{23}(CO)_{20}(PEt_3)_8$ (distorted b.c.c., see Fig. 10, *b*, *c*) clusters with similar compositions provides an example of "isomerism" of the 23-atom metal core due to a small difference in the composition of the ligand shell. This isomerism is illustrative of a flexibility of the atomic packings in large clusters, which has been noted for the first time by Chini.[22]

The histogram of the interatomic Pd—Pd distances for the $Pd_{23}(CO)_{20}(PEt_3)_8$ cluster is shown in Fig. 10, *c*.

The b.c.c. packing of metals is characterized by the fact that the second coordination sphere approaches the first coordination sphere ($\sqrt{(4/3)}a \approx 1.1a - 1.2a$ and a, respectively) as well as by the absence of the coordination spheres at $a\sqrt{2}$ and $a\sqrt{3}$ in the range of 3—4 Å. The closest sphere at $\sqrt{(4/3)}a$ is manifested as a "shoulder" shifted by 0.4—0.5 Å from the neighboring sphere. The next maximum at $\sqrt{(8/3)}a$ is shifted to distances ≥4 Å (see Fig. 10, *c*). All known b.c.c.-type clusters are characterized by strong distortions due to which the coordination spheres become broad and smeared.

3.5. Local icosahedral packing

A series of medium-sized clusters containing the metal core with the idealized I_h symmetry (centered icosahedron) were synthesized and structurally characterized (see Fig. 4, *d*). Examples are $[Au_{13}(PMe_2Ph)_{10}Cl_2]^{3+}$,[104] $Au_{13}(dppm)_6^{4+}$ (dppm = $Ph_2PCH_2PPh_2$),[105] $Au_{12}Pd(dppe)(PPh_3)_6Cl_4$ (dppe = $PPh_2C_2H_4PPh_2$),[106] $Au_{12}Pd(PPh_3)_8Cl_4$,[107] $[Au_9Cu_4(PPh_2Me)_8Cl_8]^+$,[108] and $[Au_9Ag_4(PPh_2Me)_8Cl_8]^+$.[109] The fragment of the centered icosahedron is present also in the larger carbonyl phosphine clusters $Pd_{16}(CO)_{13}(PEt_3)_9$[110] and $Pt_{17}(CO)_{12}(PEt_3)_8$.[111] In other carbonyl clusters, such as $[Pt_{19}(CO)_{22}]^{4-}$ [41] and $[Rh_{15}(CO)_{28}(C)_2]^-$,[112] the central atom is surrounded by 12 atoms, which form a pentagonal prism with two caps above the pentagonal faces.

Crystal lattices with a translational symmetry cannot have the C_5 symmetry axes. However, an icosahedron serves as a building block in crystals with loose atomic packings, such as certain allotropic modifications of boron and borides (see Ref. 11). In quasicrystals, *viz.*, Al-based alloys[113] and a number of other intermetallides, a special quasicrystalline long-range order without translations is observed. This type is compatible with the pentagonal local symmetry. Such quasicrystals can give X-ray diffraction patterns with the five- or tenfold symmetry axes and exhibit some other unusual properties.[114]

The pentagonal symmetry of the metal core is observed rather frequently in the large clusters listed in Table 3. The structures of such clusters can be classified into two groups. The first group includes atomic cores consisting of several condensed or interpenetrating icosahedra. The second group includes multi-shell "onions" in which the central atom is surrounded by several icosahedral shells. Examples of structures of the first type are provided by bimetallic Au—Ag clusters, a large series of which was studied by Teo and co-workers.[62] According to the results of calculations, the two-shell Mackay icosahedron is the energetically most favorable polyhedron of ligand-free 55-atom clusters.[15] This polyhedron serves as the inner core of the 145-nuclear $Pd_{145}(CO)_{60}(PEt_3)_{30}$ cluster,[97] which has been studied recently by X-ray diffraction (see below).

The 25-nuclear $[Ag_{12}Au_{13}Br_8(PPh_3)_{10}]^+SbF_6^-$ · · 20EtOH cluster[68] (Fig. 11, *a*) consists of two centered vertex-shared icosahedra. The metal core thus formed has the idealized D_{5h} point symmetry. The following structural elements are successively located along the C_5 axis passing through the centers of the two icosahedra: (1) Ag atom, (2) five-membered ring consisting of Au atoms, (3) central Au atom of the first icosahedron, (4) five-membered ring consisting of Ag atoms, (5) vertex shared by the two icosahedra, *viz.*, the Au atom, (4′) five-membered ring consisting of Ag atoms, (3′) central Au atom of the second icosahedron, (2′) five-membered ring formed by Au atoms, and (1′) Ag atom. (Within the framework of the idealized symmetry, only fragments (1)—(5) are symmetrically independent, see Fig. 11 *a*, *b*; the symmetrically related positions are primed.) In the icosahedra linked together, five-membered rings (4) and (4′) formed by Ag atoms are in an eclipsed orientation with respect to the C_5 axis. Two terminal 12-coordinate interstitial Au atoms are at the centers of the icosahedra. The central interstitial gold atom is located inside the bicapped pentagonal prism. Each exopolyhedral Au atom is coordinated by the PPh₃ ligand, and two Ag vertices on the C_5 axis are coordinated by the terminal Br atoms. The Ag atoms that form the pentagonal prism are linked by six μ_2-bridging Br atoms along five Ag—Ag lateral edges of the prism. The lengths of the bonds with the interstitial Au atom having an icosahedral environment are as follows: 2.76 Å to the Ag atom on the C_5 axis; 2.69—2.75 Å to the Au atoms that form the five-membered ring; 2.80—2.87 Å to the Ag atoms involved in the five-membered ring; 2.85 Å to the Au atom that links two icosahedra. The lengths of the bonds between the Au atom that links two icosahedra and the Ag atoms are in the range of 2.87—2.93 Å. The lengths of the bonds between the Ag atoms of two adjacent five-membered rings are in the range of 2.89—3.10 Å.

The composition of the metal core of the $[Ag_{12}Au_{13}Br_8(P(p\text{-}tol)_3)_{10}]^+PF_6^-$·10EtOH cluster[67] is identical to that of the metal core in $[Ag_{12}Au_{13}Br_8(PPh_3)_{10}]^+SbF_6^-$·20EtOH;[68] however, two initial icosahedra in the former are rotated with respect to the C_5 axis by ~36°, *i.e.*, they are in a staggered conformation (see Fig. 11, *b*) with the idealized D_{5d} symmetry. The Ag atoms involved in the five-membered rings form a pentagonal antiprism. The central Au atom that links two icosahedra has an icosahedral environment. Therefore, the core of the $[Ag_{12}Au_{13}Br_8(P(p\text{-}tol)_3)_{10}]^+$ cluster cation consists of three interpenetrating icosahedra. The lengths of the bonds between the central Au atom and the Ag atoms (2.83—2.90 Å) are somewhat shorter than those observed in the eclipsed conformation. The edges linking the two central five-membered rings consisting of Ag atoms are, on the contrary, substantially elongated
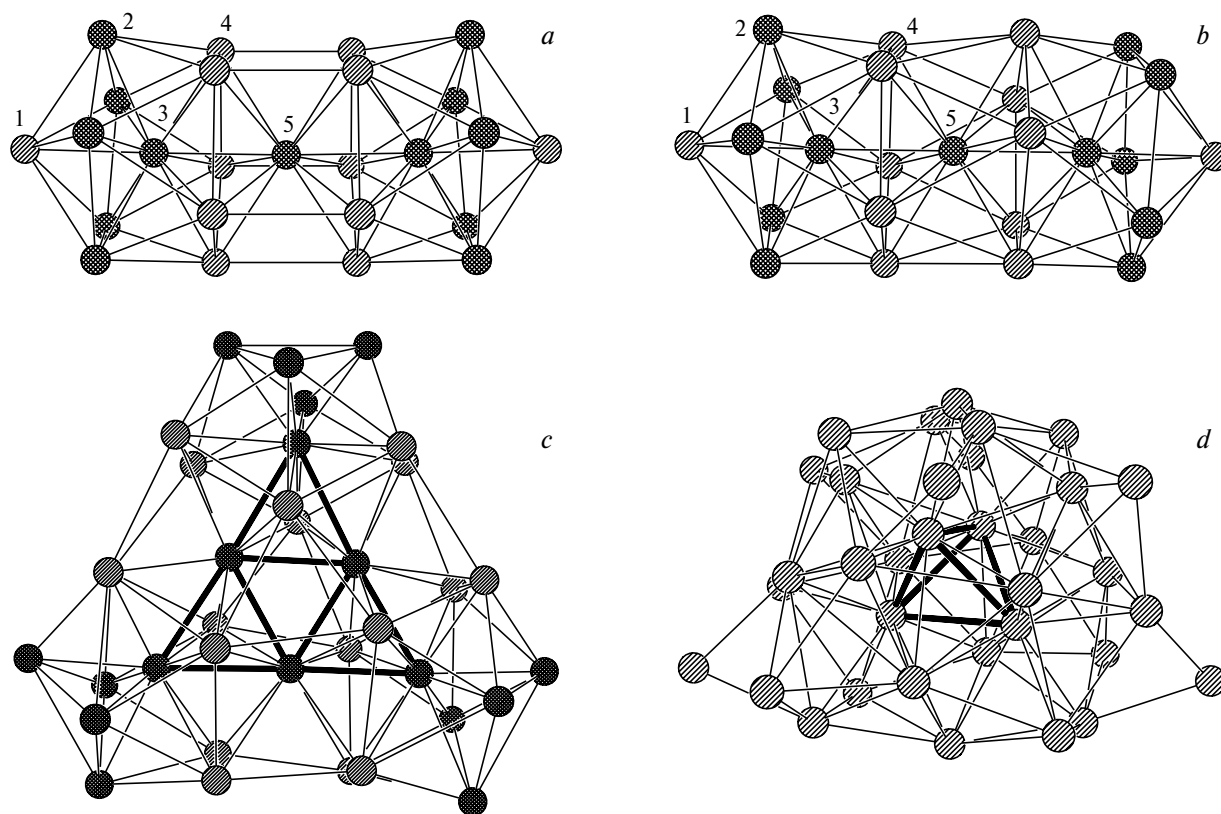
Fig. 11. Clusters based on interpenetrating icosahedra: (*a*) $[Ag_{12}Au_{13}Br_8(PPh_3)_{10}]^{+}$,[68] (*b*) $[Ag_{12}Au_{13}Br_8(P(p\text{-tol})_3)_{10}]^{+}$,[67] (*c*) $Ag_{20}Au_{18}Cl_{14}(P(p\text{-tol})_3)_{12}$,[80,81] and (*d*) $Pd_{34}(CO)_{24}(PEt_3)_{12}$.[76] In Figs. *a* and *b*, the partition of the symmetrically independent part of the metal polyhedron is denoted by numbers (see the text); in Figs. *c* and *d*, the interstitial fragments are marked off.

(3.19—3.29 Å). Six μ_2-Br ligands are coordinated along five of these Ag—Ag bonds.

All 12 structurally characterized 25-nuclear biicosahedral clusters are presented in Table 4. In seven of these clusters, two icosahedral fragments adopt an eclipsed conformation. In three clusters, two icosahedral fragments are, by contrast, in a staggered conformation. In the $\{Ag_{12}Au_{13}Cl_7[P(p\text{-tol})_3]_{10}\}^{2+}$ [63] and $\{Ag_{12}Au_{13}Cl_8[P(p\text{-tol})_3]_{10}\}^{+}$ clusters,[65] the icosahedra are rotated with respect to each other by ~15°. In the $[Ag_{12}Au_{13}Br_8(PPh_3)_{10}]^{+}Br^{-}\cdot$ $\cdot 3EtOH$ cluster[69] adopting a distorted staggered conformation, three interstitial Au atoms are not in a straight

Table 4. The 25-nuclear Ag—Au clusters with a local icosahedral environment of the metal atoms*

Cluster	Orientation of icosahedra	Positions of atoms in the cluster					Equatorial ligands	Reference
		1	2	3	4	5		
$[Ag_{12}Au_{12}NiCl_7(PPh_3)_{10}]^{+}SbF_6^{-}\cdot 15EtOH$	Eclipsed	Ag	Au	Au/Ni	Ag	Au	5 μ_2-Cl	59
$[Ag_{12}Au_{12}PtCl_7(PPh_3)_{10}]^{+}Cl^{-}$	Eclipsed	Ag	Au	Au/Pt	Ag	Au	5 μ_2-Cl	60
$Ag_{13}Au_{10}Pt_2Cl_7(PPh_3)_{10}\cdot 10Et_2O$	Eclipsed	Ag	Au	Pt	Ag	Ag	5 μ_2-Cl	61
$Ag_{13}Au_{10}Pd_2Cl_7(PPh_3)_{10}$	Eclipsed	Ag	Au	Pd	Ag	Ag	5 μ_2-Cl	62
$Ag_{13}Au_{10}Ni_2Cl_7(PPh_3)_{10}$	Eclipsed	Ag	Au	Ni	Ag	Ag	5 μ_2-Cl	62
$\{Ag_{12}Au_{13}Cl_7[P(p\text{-tol})_3]_{10}\}^{2+}[SbF_6^{-}]_2\cdot xEtOH$	Skewed by ~15°	Ag	Au	Au	Ag	Au	5 μ_2-Cl	63
$[Ag_{12}Au_{13}Cl_8(PMe_3)_{10}]^{+}SbF_6^{-}$	Eclipsed	Ag	Au	Au	Ag	Au	5 μ_2-Cl, 1 μ_4-Cl	64
$\{Ag_{12}Au_{13}Cl_8[P(p\text{-tol})_3]_{10}\}^{+}PF_6^{-}$	Skewed by ~15°	Ag	Au	Au	Ag	Au	4 μ_2-Cl, 2 μ_3-Cl	65
$[Ag_{12}Au_{13}Br_8(PPh_3)_{10}]^{+}Br^{-}$	Staggered	Ag	Au	Au	Ag	Au	4 μ_2-Br, 2 μ_3-Br	66
$\{Ag_{12}Au_{13}Br_8[P(p\text{-tol})_3]_{10}\}^{+}PF_6^{-}\cdot 10EtOH$	Staggered	Ag	Au	Au	Ag	Au	6 μ_2-Br	67
$[Ag_{12}Au_{13}Br_8(PPh_3)_{10}]^{+}SbF_6^{-}\cdot 20EtOH$	Eclipsed	Ag	Au	Au	Ag	Au	6 μ_2-Br	68
$[Ag_{12}Au_{13}Br_8(PPh_3)_{10}]^{+}Br^{-}\cdot 3EtOH$	Staggered	Ag	Au	Au	Ag	Au	4 μ_2-Br, 2 μ_3-Br	69

* The numbering scheme for the positions in the metal core is presented in Fig. 11 *a, b*.

line. The distances along the edges, which link two five-membered rings formed by Ag atoms, vary from 3.05 to 3.41 Å. By contrast, in the $[Ag_{12}Au_{13}Br_8(PPh_3)_{10}]^+Br^-$ cluster[66] with an analogous composition, whose crystals contain no molecules of solvation, the icosahedral fragments adopt a symmetrical staggered conformation. Therefore, the biicosahedral clusters are structurally non-rigid and can change their geometry under the influence of the packing forces.

The structures of biicosahedral clusters have been analyzed in the review.[62] In the trimetallic Au—Ag—M clusters, Group 10 metals (M = Pt, Pd, Ni) occupy predominantly positions at the centers of fused icosahedra due to large bond energies of their atoms in the bulk metals (M > Au > Ag). The Ag atoms occupy terminal vertices (1) and (1′) as well as positions (4) and (4′) in the equatorial plane. The more electronegative Au atoms are generally coordinated by phosphine ligands. The Ag atoms are coordinated by halogen ligands. Therefore, the surface of the cluster core can be enriched with atoms of particular elements by varying the ligand environment. The authors of the cited review[62] used the notions of rotamerism (rotational isomerism that occurs in the case of different mutual orientations of two icosahedra) and rouletta-merism, which characterizes the orientation of the metal core within the five- or six-membered ring formed by halogen ligands, for the description of structures of biicosahedral clusters.

Two clusters with composition $Ag_{20}Au_{18}Cl_{14}(P(p\text{-}tol)_3)_{12}$ (see Fig. 11, *c*),[80,81] which differ in the number of molecules of solvation in the crystal, and the $[Ag_{20}Au_{18}Cl_{12}(PPh_3)_{14}]^{2+}$ cluster cation have more complex structures.[82] All these compounds contain isostructural 36-atom metal cores to which two exopolyhedral Ag atoms are linked through the Cl bridging atoms. The metal core of $Ag_{20}Au_{18}Cl_{14}(P(p\text{-}tol)_3)_{12}$[80] with the idealized D_{3h} symmetry can be represented as three centered icosahedra linked in pairs through shared vertices. The cluster contains six interstitial Au atoms, which form a ν_3 triangle with the edge lengths varying in the range of 2.70—2.92 Å. Three interstitial atoms, which link the icosahedra, have a 12-atom closest environment, which can be described as a bicapped pentagonal prism formed by eight Ag atoms and four Au atoms. The distances from the "intericosahedral" Au atoms to the Ag atoms are in the range of 2.79—3.11 Å and to the Au atoms at the centers of the icosahedra are in the range of 2.76—2.93 Å. The exopolyhedral Au atoms are coordinated by the phosphine ligands. The Ag atoms are coordinated by the bridging Cl atoms.

The $[Ag_{19}Au_{18}Br_{14}(P(p\text{-}tol)_3)_{12}]^{2+}$ cluster cation[83] contains the same 36-atom metal core but has only one exopolyhedral Ag atom linked through the bridging Br atoms. The centers of the icosahedra are shifted in the opposite direction with respect to the plane formed by

three linking Au atoms. Therefore, a mixed "icosahedron/pentagonal prism" type of close packing is often observed in a series of clusters with the pentagonal local symmetry of the atomic environment. This packing mode can be considered as an analog of the above-mentioned mixed f.c.c./h.c.p. packing in carbonyl clusters. However, this packing mode, unlike the f.c.c./h.c.p. packing, is characterized by the absence of planar atomic layers.

The metal core of the $Pd_{34}(CO)_{24}(PEt_3)_{12}$ cluster[76] (see Fig. 11, *d*) consists of four distorted interpenetrating icosahedra. Four interstitial Pd atoms form the inner tetrahedron with the edge lengths varying in the range of 2.59—2.68 Å. The average Pd—Pd distance in the tetrahedron (2.64 Å) is substantially shorter than that in bulk Pd metal (2.75 Å). In the tetrahedron, each Pd atom is in a distorted icosahedral environment formed by 12 Pd atoms. The coordination environments of the interstitial Pd atoms are icosahedra without one edge that together form the second coordination sphere consisting of 22 Pd atoms around the initial tetrahedron. The distances from the four interstitial Pd atoms to the outer sphere composed of 22 Pd atoms are in the range of 2.63—2.98 Å. Two μ_2-coordinated Pd atoms are bound to the 26-atom core consisting of four icosahedra fused along the Pd—Pd bonds. Two μ_3- and four μ_4-coordinated Pd atoms are bound to the square faces. The entire Pd_{34} metal core is surrounded by the phosphine and bridging carbonyl ligands.

The $[Pd_{29}Ni_3(CO)_{40}]^{4-}$ cluster anion[75] is also built from four interpenetrating icosahedra, whose centers form the inner tetrahedron. The $Pd_{35}(CO)_{23}(PMe_3)_{15}$ and $Pd_{39}(CO)_{23}(PMe_3)_{16}$ clusters consist of five distorted interpenetrating icosahedra, whose centers form a trigonal bipyramid.[75]

The radial distribution histogram for the 34-atom metal core in the $Pd_{34}(CO)_{24}(PEt_3)_{12}$ cluster along with the partial distributions of interatomic distances in the local environment of four interstitial and 30 exopolyhedral Pd atoms are shown in Fig. 12. The ideal centered icosahedron assembled from rigid spheres with diameters *a* is characterized by the absence of the coordination sphere at $a\sqrt{2}$ as well as by splitting of the nearest sphere into the center—vertex (*a*) and vertex—vertex contacts (along the edge of the icosahedron, 1.052*a*). However, in all icosahedral clusters studied by X-ray diffraction, the coordination spheres are broadened, and, hence, the components at *a* and 1.052*a* coalesce into one closest sphere. The weak maxima at distances of ~4 Å reflect the contribution of the pentagonal-prismatic environment. The absence of the sphere at $a\sqrt{2}$ along with a pronounced sphere at ~$a\sqrt{3}$ in RDF can be considered as an indication of an icosahedral packing. The local icosahedral packing differs from the b.c.c. packing, which gives a similar histogram (see Fig. 10, *c*), by the absence of a "shoulder" of the first coordination sphere at ~1.1—1.2*a*.
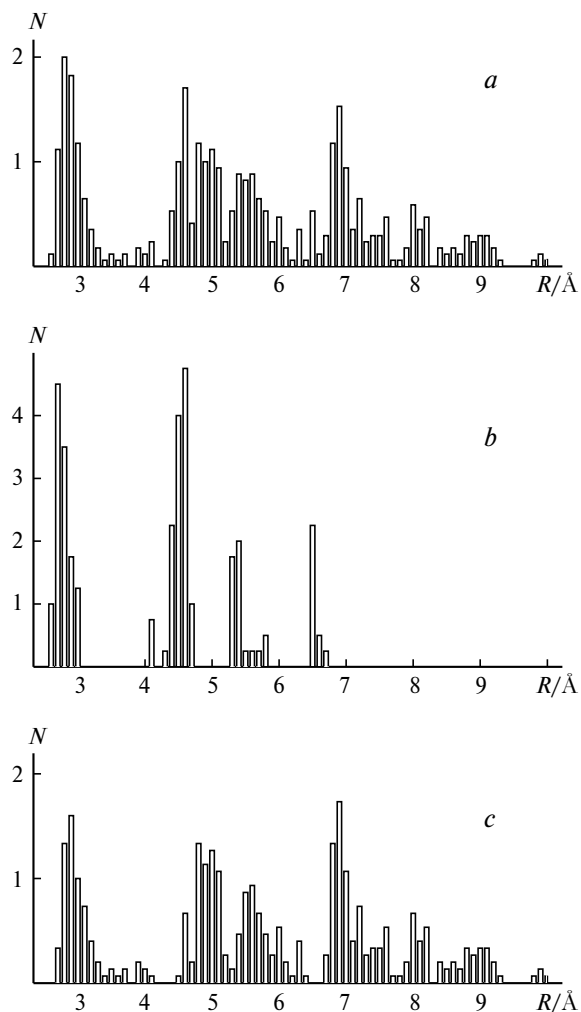
Fig. 12. Histograms of the Pd—Pd interatomic distances in the $Pd_{34}(CO)_{24}(PEt_3)_{12}$ cluster:[76] (*a*) all metal atoms, (*b*) environment of four interstitial Pd atoms, and (*c*) all atoms of the Pd_{30} shell.

An enlargement of the metal core based on interpenetrating icosahedra leads to an increase in strains and smearing of maxima in the histograms (see, for example, Refs. 36 and 37). Broad coordination spheres of the Pd_{34} core (see Fig. 12, *a*) are split into sharper maxima corresponding to the partial distributions of the distances in the environment of four interstitial Pd atoms (where the spheres are shifted by 0.10—0.15 Å to shorter distances, see Fig. 12, *b*) and broadened spheres of the distorted 30-atom periphery (see Fig. 12, *c*). A comparison of the positions of the maxima shown in Fig. 12, *b* and *c* demonstrates that the icosahedral environment, in which the distances between the vertices of the icosahedron are somewhat longer than the equilibrium shortest M—M distances, leads to contraction of the interstitial metal atoms.

Presumably, it is an increase in destabilizing strains with increasing size of the clusters of this type that is responsible for the lack of the 45-atom pentagon dodecahedron, in which all pentagonal faces are capped and which contains the inner centered icosahedral core with all atoms being in the icosahedral closest environment, among the structurally studied clusters.[14,37] Structural data on clusters based on the 127-atom icosahedron consisting of vertex-shared centered icosahedra are also lacking. However, this fractal algorithm proposed in the review[62] can, presumably, take place in assembling quasicrystals.[114]

The $Pd_{69}(CO)_{36}(PEt_3)_{18}$ cluster[96] in which the central Pd_{15} core is surrounded by the Pd_{54} "shell" (Fig. 13) is the largest structurally characterized cluster consisting of interpenetrating icosahedra. Three of 15 interstitial atoms occupy the centers of three icosahedra linked by shared triangular faces. The remaining 12 interstitial Pd atoms are in a distorted icosahedral environment. Therefore, the inner 15-atom core can be described as the centered icosahedron Pd_{13} in which two opposite faces are capped. The radial binding Pd—Pd distances in the icosahedral environment (2.66—2.70 Å for the central atom; 2.70—2.73 Å for the caps in the Pd_{15} core) demonstrate a characteristic shortening by 5% compared to the average edge lengths in the icosahedron (2.82 and 2.86 Å, respectively; the tangential distances vary in the range of 2.66—3.13 Å).
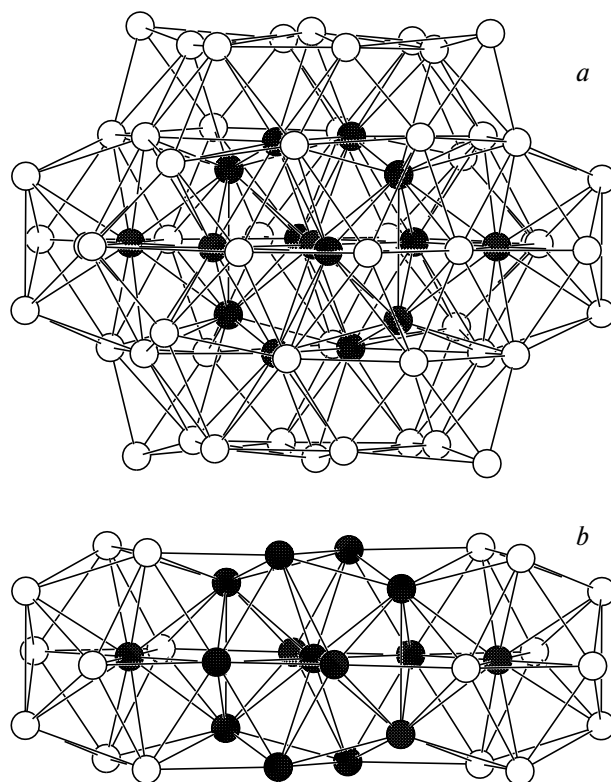
Fig. 13. Structure of the metal core in the $Pd_{69}(CO)_{36}(PEt_3)_{18}$ cluster:[96] (*a*) overall view of the cluster without ligands, (*b*) central 33-atom fragment (three face-shared icosahedra) surrounded by the 36-atom cylindrical shell. The interstitial Pd_{15} fragment marked off.

The Pd_{69} metal core also has five loose hexagonal layers (9:13:19:13:9) containing four additional Pd atoms, which are located between the inner layers, and two metal atoms serving as caps. This cluster with a diameter of 1.4 nm is, apparently, intermediate between the local icosahedral and distorted multilayer packings of the metal atoms. The latter becomes energetically favorable as the size of the metal core increases.

The 145-nuclear $Pd_{145}(CO)_{60}(PEt_3)_{30}$ cluster is the unique example of multi-shell icosahedral clusters. This cluster is the largest homoatomic cluster studied by single-crystal X-ray diffraction (Fig. 14, *a*) so far. The metal core of this remarkable compound[97] consists of the central Pd atom surrounded by three nested coordination spheres formed by 12, 45, and 60 Pd atoms. In the cited study,[97] isostructural 145-nuclear clusters with the PMe_3 and PPh_3 ligands were also mentioned.

The first sphere about the central atom in the 145-atom metal core is an icosahedron formed by 12 Pd atoms (see Fig. 14, *b*). The second icosahedral shell consisting of 42 atoms is formed by superimposing the six-atom v_2-triangular face onto each v_1-triangular face of the inner centered Pd_{13} icosahedron. Therefore, the inner 55-atom core (two-shell Mackay icosahedron) can be composed of 20 slightly distorted v_2 tetrahedra with a shared vertex at the center of the cluster.

According to Mackay, the formation of the third coordination sphere requires the arrangement of v_3 triangles above each v_2-triangular face of the second sphere. However, the third sphere in the Pd_{145} metal core (see Fig. 14, *c*) consists of 60 atoms and is an "isomer" of fullerene C_{60} referred to as the rhombotruncated icosadodecahedron (3,4,5,4). This Archimedean polyhedron contains 60 equivalent vertices, 12 pentagonal faces, 20 triangular faces, and 30 square faces. In the study,[97] it was hypothesized that the formation of such an unusual sphere is determined by two tendencies, *viz.*, the maximization of the coordination numbers for the atoms located inside the cluster and the minimization of the number of atoms on the surface of the metal core. The square faces of the third metal shell are capped with 30 Pd atoms, each being coordinated by one PEt_3 ligand and, presumably, two μ_2-CO ligands.

The histograms of the interatomic Pd—Pd distances in the two-shell icosahedral Pd_{55} core and in the entire $Pd_{145}(CO)_{60}(PEt_3)_{30}$ cluster are shown in Figs. 15, *a* and *b*, respectively. In a multi-shell Mackay icosahedron, the following types of the local environment are present simultaneously:[36] (1) f.c.c. packing (cuboctahedron) for atoms inside 20 tetrahedral "domains," which are bounded by the center and a triangular face of the icosahedron, (2) h.c.p. packing (twinned cuboctahedron) for atoms at the interface of two domains, (3) bicapped pentagonal prismatic environment of atoms located inside the icosahedron on its body diagonals, and (4) icosahedral envi-
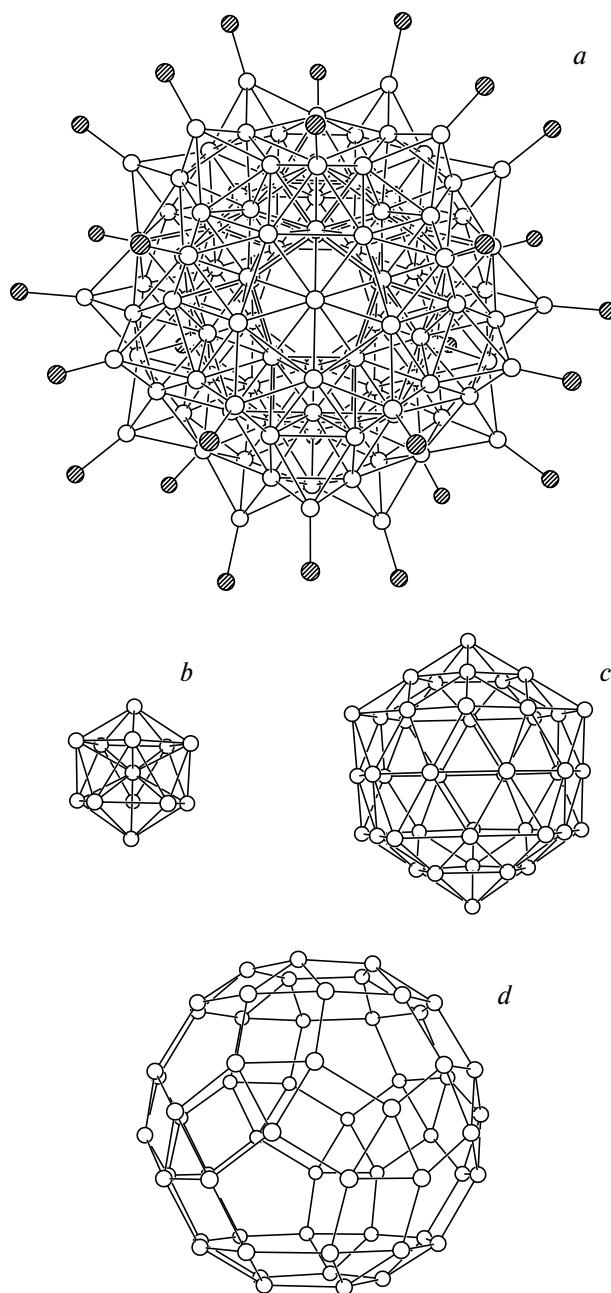
Fig. 14. Multi-shell structure of the metal core of $Pd_{145}(CO)_{60}(PEt_3)_{30}$.[97] (*a*) overall view of the cluster without CO ligands, the P atoms of the phosphine ligands are dashed, (*b*) inner centered icosahedron Pd_{13}, (*c*) second icosahedral 42-atom shell, and (*d*) third 60-atom shell.

ronment of the only central atom. The histograms (see Fig. 15) represent superpositions of coordination spheres typical of these packings and are indicative of substantial distortions of the outer metal shell of the cluster. Thus, the RDF for the inner core Pd_{55} shows that the closest f.c.c. and h.c.p. spheres are clearly separated. However, the first maximum at distances of 2.65—2.95 Å is broadened. The contribution of the distorted environment to
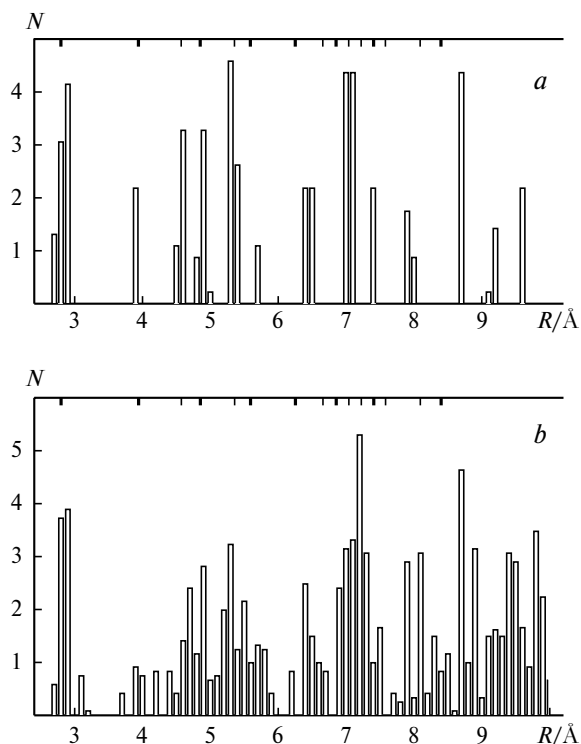
Fig. 15. Histograms of the M—M interatomic distances in the $Pd_{145}(CO)_{60}(PEt_3)_{30}$ cluster:[97] (*a*) icosahedral Pd_{55} core and (*b*) total Pd_{145} metal core. The idealized coordination spheres specific for h.c.p. are shown by thin dashes at the top of the plot; the coordination spheres common to h.c.p. and f.c.c. (normalized to the average distance $R = a$) are indicated by bold dashes.

the outer 60-atom shell leads to coalescence of the adjacent coordination spheres giving rise to broad maxima. The histogram in Fig. 15, *b* demonstrates that the Mackay icosahedra, like other clusters with a mixed atomic packing, are difficult to identify based on the one-dimensional experimental radial distribution functions without resort to additional data (see Section 4). The average Pd—Pd distances in the metal core increase from 2.63 Å (at the central atom) to 3.09 Å (in the five-membered rings of the third 60-atom sphere), which is indicative of a radial contraction of the inner part of the cluster.

3.6 "Amorphous" clusters

In a number of clusters, the metal cores cannot be described in terms of a regular crystal packing of metals, and the local environment of the interstitial atoms does not have the pentagonal symmetry. A range of the closest M—M contacts in such clusters is generally broadened, and the histograms of interatomic distances have no pronounced maxima beyond the first metal—metal coordination sphere. We called this strongly distorted type of atomic packing an "amorphous" packing.[84] The distorted b.c.c.-type metal cores and distorted polyicosahedral clusters are similar to "amorphous" clusters in the degree of
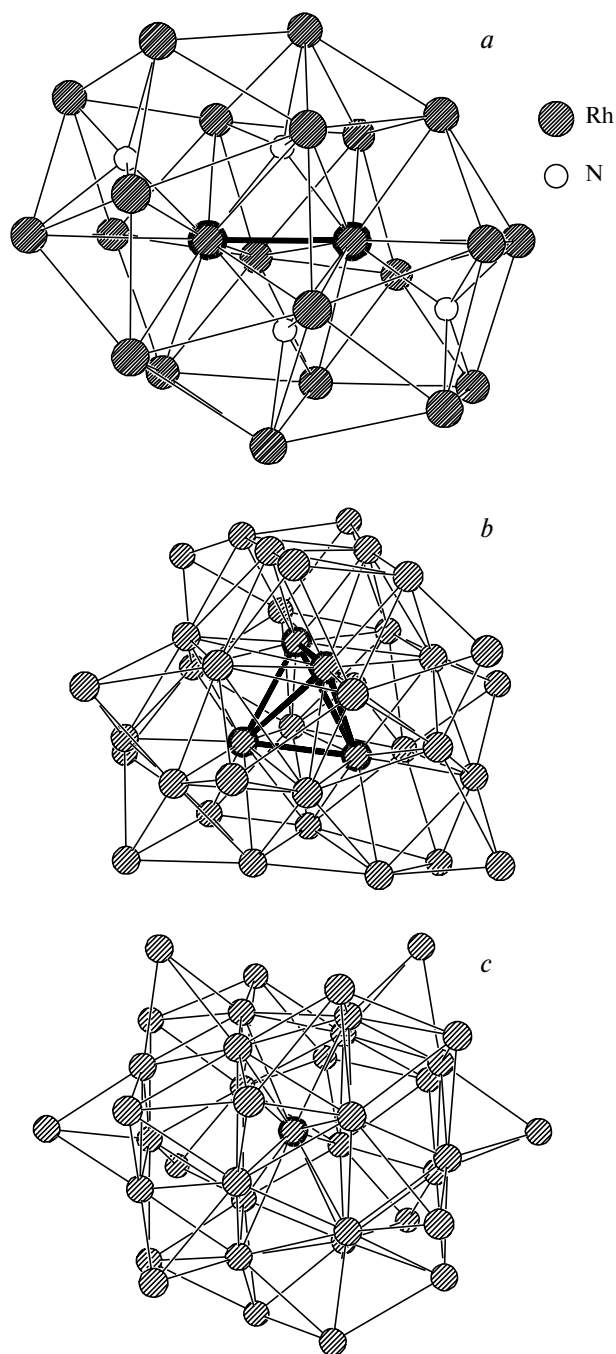
Fig. 16. Structures of the clusters with an "amorphous" atomic packing: (*a*) $[Rh_{23}(CO)_{38}N_4]^-$,[54] (*b*) $Pd_{38}(CO)_{28}(PEt_3)_{12}$,[84] and (*c*) $[Au_{39}Cl_6(PPh_3)_{14}]^{2+}$.[87] The interstitial metal atoms are marked off.

disorder of their local atomic environment. The structures of selected "amorphous" clusters are shown in Fig. 16.

One of the simplest examples of an "amorphous" packing is the $[Rh_{23}(CO)_{38}N_4]^-$ cluster anion,[54] which contains two interstitial Rh atoms at a distance of 2.57 Å from each other and has four μ_5-coordinated interstitial N atoms (see Fig. 16, *a*). The overall coordination environment of

the two interstitial Rh atoms consists of 13 Rh atoms at distances of 2.75—3.06 Å. Four μ_4- and two μ_5-coordinated Rh atoms are bound to the above-mentioned atoms. The metal core is additionally coordinated by the bridging and terminal CO ligands.

The metal skeletons in the $[HNi_{34}(CO)_{38}C_4]^{5-}$ and $[Ni_{35}(CO)_{39}C_4]^{6-}$ cluster anions[77] consist of the three-layer f.c.c. Ni_{20} core (8:4:8 atoms). Four interstitial C atoms are bound to the square faces of the Ni_{20} fragment. The remaining Ni atoms are attached to the $Ni_{20}C_4$ fragment to form its distorted metal shell. The clusters contain four interstitial Ni atoms in a distorted cuboctahedral environment, which form the middle layer of an f.c.c. fragment. The cluster cores are coordinated by the terminal and bridging CO ligands. Therefore, these clusters are related to the above-considered f.c.c. polyhedra. However, the packing of their exopolyhedral atoms is deformed due to the insertion of the carbide C atoms into the octahedral cavities.

The $[Ni_{31}Sb_4(CO)_{40}]^{6-}$ cluster[78] with the idealized C_2 symmetry has two interstitial Ni atoms. Each of these atoms is surrounded by nine Ni atoms (2.47—2.90 Å) and three Sb atoms (2.50—2.68 Å). However, the Ni_9Sb_3 polyhedron cannot be described as a fragment of a particular close packing. The exopolyhedral Ni atoms are coordinated by the bridging and terminal CO ligands. In this polyhedron, distortions of the packing are particularly pronounced in the inner core, which is similar in composition to binary metal pnictide phases.

The homoatomic metal core of the $Pd_{38}(CO)_{28}(PEt_3)_{12}$ cluster[84] has the idealized D_2 symmetry (see Fig. 16, *b*) and contains four interstitial Pd atoms. The interstitial metal atoms form a distorted tetrahedron with two long (2.958 and 2.970 Å) and four short (2.51—2.61 Å) Pd—Pd bonds. Each interstitial atom is surrounded by 12 Pd atoms at distances of 2.51—3.31 Å to form a shell consisting of 22 Pd atoms around the initial tetrahedron. The interstitial Pd atoms together with 20 Pd atoms of this shell form nearly planar layers (4:8:8:4 atoms), which are irregularly arranged one above another. The cluster is capped with twelve $PdPEt_3$ groups (in two of which the PEt_3 ligands are rotationally disordered) and coordinated by the bridging carbonyl ligands. The average shortest Pd—Pd distance in the cluster (2.78 Å) is close to that observed in the bulk metal (see Table 1).

The $[HNi_{38}(CO)_{42}C_6]^{5-}$ cluster anion[86] contains the $Ni_{38}C_6$ core with the D_{3d} symmetry. Eight Ni atoms form the inner cube with the average Ni—Ni distance of 2.40 Å. Each face of this cube is coordinated by the carbide C atom, to which four more Ni atoms are bound thus forming the square antiprism. Twenty four exopolyhedral Ni atoms form a truncated octahedron around the inner Ni_8 cube. The $Ni_{32}C_6$ fragment resembles an "hollow" 32-atom shell, which can be described as a ν_3-octahedron without vertices similar to that observed in the f.c.c.-type

$[Ni_{24}Pt_{14}(CO)_{44}]^{2-}$ [57] and $[Pt_{38}(CO)_{44}]^{2-}$ clusters[58] (see Section 3.1). However, the atoms of eight hexagonal faces in the cluster under consideration are "pressed" into the metal core. Six μ_3-Ni caps are additionally bound to this metal carbide fragment (aver. Ni—Ni, 2.49 Å) according to the idealized D_{3d} symmetry. The ligand shell of the cluster consists of eight terminal and 34 μ_2-bridging CO ligands.

Each interstitial Ni atom of the cluster is surrounded by ten Ni atoms and three carbide C atoms. In spite of a regular arrangement of the $Ni_{38}C_6$ cluster core, which resembles a fragment of the crystal lattice of chromium carbide $Cr_{23}C_6$, the Ni—Ni distances in this core vary over a wide range, and their average values increase from 2.40 Å (in the central cube) to 2.63 Å (between the bases of the tetragonal antiprism formed by the carbide C atoms). Therefore, a distorted "amorphous" packing is often observed in the cluster cores containing interstitial light atoms (C, N). These cluster structures containing guest atoms are, apparently, intermediate between compact metal cores and large binary clusters, which are beyond the scope of our review.

The metal core in the $[Au_{39}Cl_6(PPh_3)_{14}]^{2+}$ cluster cation[87] (see Fig. 16, *c*) with the C_3 point symmetry consists of four layers (6:9:9:6). The outer hexatomic layers can be described as ν_2 triangles; the Au—Au distances within the layer are in the range of 2.73—2.92 Å. The inner layers consisting of nine atoms are ν_3 triangles without the central atom, which are rotated along the C_3 axis by ~30° with respect to each other. The only interstitial Au atom is located between these layers on the C_3 axis. This atom is surrounded by two six-membered rings formed by Au atoms of the inner layers analogously to sandwich compounds; the corresponding distances are in the range of 2.98—3.11 Å. The distances between the vertices of the ν_3 triangles, which are rotated by 30° with respect to each other, are in the range of 3.01—3.07 Å. Eight $AuPPh_3$ caps are additionally coordinated to the triangular faces of the metal core. The remaining six PPh_3 ligands are coordinated to the Au atoms and are located at the vertices of the ν_3 triangles. The chloride ligands coordinated to the Au atoms are located at the vertices of the ν_2 triangles.

The $Pd_{59}(CO)_{32}(PMe_3)_{21}$ cluster is the largest known "amorphous" cluster studied by X-ray diffraction analysis.[75] The core of this cluster with the D_3 symmetry has the shape of an ellipsoid with a long axis of 1.2 nm and contains 11 interstitial Pd atoms. The inner Pd_{11} core consists of two face-shared octahedra with the two opposite most remote triangular faces being capped. Two inner Pd caps have an icosahedral environment formed by 12 Pd atoms, whereas the middle portion of the cluster corresponds to a strongly distorted "amorphous" packing. It should be noted that fusion of the centered icosahedral fragments with other polyhedra in this cluster is inconsis-

tent with the mechanism of fusion of icosahedra through shared vertices proposed in the study.[62]

The histograms of the metal—metal distances for "amorphous" clusters show strong distortions of the coordination spheres. Such clusters have continuous distributions of the metal—metal distances at $R > 4$ Å with broad maxima about $R \approx 2a$ and $R \approx 3a$ (a is the average distance to the first pronounced coordination sphere).* Distortions of the packing are accompanied by a decrease in the average coordination numbers in each sphere. This type of distributions, which resemble RDF for liquids,[115] justifies the term "amorphous" as applied to a distorted atomic packing *inside* the clusters. The latter can form high-quality molecular crystals (for example, the H atoms of the ordered PEt_3 ligands were revealed in the structure of $Pd_{38}(CO)_{28}(PEt_3)_{12}$, see Ref. 84). It should be noted that the related $Pd_{34}(CO)_{24}(PEt_3)_{12}$ cluster of the icosahedral type contains no planar atomic layers in the metal core. An example of RDF of the "amorphous" Pd_{38} cluster is considered in Section 4.

3.7. "Shell" clusters

Some large metal clusters are characterized by a loose atomic packing, which is not typical of the majority of compounds of this class. Small and medium-sized clusters with a loose packing of metal atoms sometimes exist as planar structures,[18,116] whereas large clusters can have a "shell" structure with guest atoms in the cavity of the large metal polyhedron. Most of cluster molecules and ions consisting of light atoms have shell polyhedral structures (cubane C_8H_8, dodecahedrane $C_{20}H_{20}$, carboranes $C_2B_{10}H_{12}$, fullerenes C_{60} and C_{70}, *etc.*). In endohedral fullerene derivatives, such as $C_{60}@Kr$,[117] $C_{80}@Sc_3N$,[118] *etc.*, guest fragments (@) are inserted into the carbon shell. The interactions of the endohedral fragments with the carbon shell are generally weaker than the strong C—C chemical bonds between the atoms of the shell. The large polyoxomolybdate clusters studied by A. Müller and co-workers[40] also belong to "shell" clusters. The cavities in the metal oxide cores of these clusters are occupied by water molecules.

For transition metal clusters, hollow shell structures are not typical, although there are numerous examples of octahedral and larger metal cores containing covalently bound nonmetal atoms in the inner cavity.[116] The bimetallic 14-nuclear cluster $\{Ag_8Ni_6[SCMe_2CH(NH_2)COO]_{12}@Cl\}^{5-}$ provides an example of medium-sized shell-type clusters. In this cluster, the chloride anion is located inside the cube formed by Ag atoms with the edge of 3.48 Å (aver.). The cube is capped with six Ni atoms (see Fig. 3, *c*) and coordinated by twelve bridging d-penicillaminate ligands.[119] Based on

the formal charge count in this cluster, the latter can be considered as composed of the Ag^I and Ni^{II} cations.

The $Ag_{45}(PPh)_{18}(PhPSiMe_3)_2Cl_7(PPr^n_3)_{12}$ and $Ag_{50}(PPh)_{20}Cl_7P(PPr^n_3)_{13}$ clusters[95] serve as examples of large "shell" clusters. Using notations accepted for endohedral derivatives, their formulas should be written as $Ag_{44}(PPh)_{18}(PhPSiMe_3)_2Cl_5(PPr^n_3)_{12}@AgCl_2$ and $Ag_{48}(PPh)_{20}Cl_5(PPr^n_3)_{13}@Ag_2PCl_2$, respectively. Based on the standard electron count in the cluster core, the guest fragments can be considered as the anions ($[AgCl_2]^-$ and $[ClAgPAgCl]^{3-}$, respectively), and all silver atoms in the core are in the oxidation state +1. Therefore, these structures are similar to the binary metal pnictide clusters related to chalcogenide derivatives of silver[39] mentioned in Section 2.

The metal core in $Ag_{44}(PPh)_{18}(PPhSiMe_3)_2Cl_5(PPr^n_3)_{12}@AgCl_2$ can be described as a 44-atom distorted elongated ellipsoid consisting of three-, four-, five-, and six-membered metallocycles (Fig. 17, *a*). The Ag—Ag shortest distances are in the range of 2.76—3.30 Å (average distance is 2.97 Å; *cf.* 2.89 Å in bulk Ag metal). The metal core is coordinated by twelve PPr^n_3 ligands, two bridging μ_2-$P(SiMe_3)Ph$ ligands, and four μ_2-Cl-ligands. The four-, five-, and six-membered rings consisting of the Ag atoms of the metal core are coordinated by six μ_4- and 12 μ_5-PPh ligands. An unusual
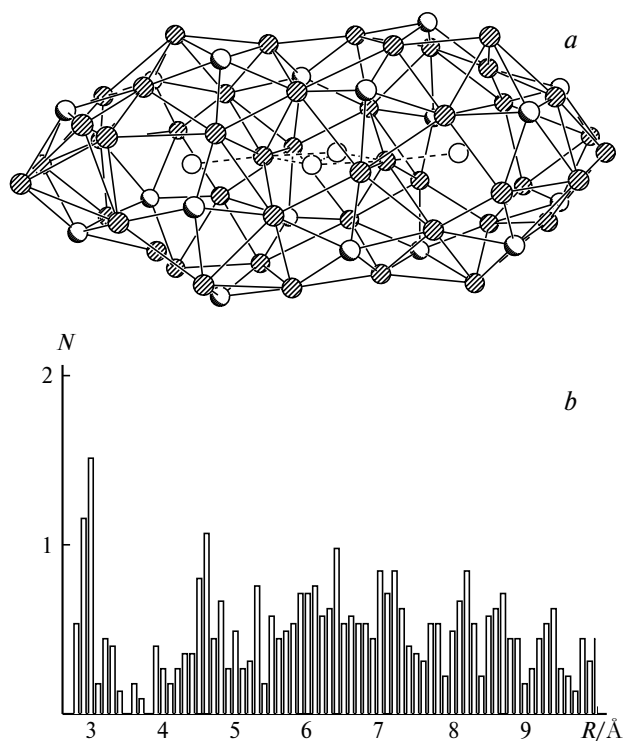
Fig. 17. Structure (*a*) and the histogram of the Ag—Ag distances (*b*) of the shell cluster $Ag_{44}(PPh)_{18}(PhPSiMe_3)_2Cl_5(PPr^n_3)_{12}@AgCl_2$.[95] The disordered positions of the Cl atoms inside the polyhedron are represented by empty circles.

---

* Unlike $Pd_{34}(CO)_{24}(PEt_3)_{12}$ (see Fig. 12, *b*), no far spheres are revealed in the "partial" environment of four interstitial palladium atoms in the 38-nuclear core.

flattened hexagonal closest environment formed by four Ag atoms and two P atoms is observed for a number of exopolyhedral Ag atoms coordinated by two μ_4- or μ_5-PPh ligands. The cavity of the metal core is occupied by the only $[AgCl_2]^-$ anionic fragment (Ag—Cl, 2.294 and 2.335 Å) disordered over two orientations with one-half occupancies. The inner Ag atom forms contacts with five Ag atoms of the shell at distances of 3.02—3.30 Å. The histograms of the Ag—Ag interatomic distances (see Fig. 17, *b*) do not reveal even broad maxima at distances >3 Å in the Ag_{44} shell, which is indicative of the absence of the local order in the packing of metal atoms.

The metal core of the $Ag_{48}(PPh)_{20}Cl_5(PPr^n_3)_{13}@Ag_2PCl_2$ cluster has an analogous structure. Its outer shell is formed by 48 Ag atoms coordinated by the terminal Pr^n_3P and bridging μ_2-Cl ligands as well as by the μ_4- and μ_5-PPh ligands. The Cl—Ag—P—Ag—Cl anionic fragment is located inside the cluster. One of the interstitial Ag atoms is surrounded by six Ag atoms of the shell at distances of 2.88—3.25 Å, whereas the second interstitial Ag atom is surrounded by five Ag atoms of the shell at distances of 3.00—3.43 Å. The above-considered compounds, which do not possess a close atomic packing, are at the boundary of a class of large metal clusters.

4. Atomic radial distribution function in structural studies of nonstoichiometric nanoparticles

As was demonstrated above, the radial distribution histograms, which are calculated for large stoichiometric clusters based on their crystal structures, provide additional possibilities for analyzing the atomic packings in metal polyhedra. For compounds, which do not form crystals, the experimental radial distribution functions (RDF) can be determined by EXAFS spectroscopy[120] and diffraction methods.[121] The lack of single-crystal X-ray diffraction data for nonstoichiometric clusters and nanoparticles increases the role of the above methods in structural studies. A comparison of the calculated radial distribution histograms for large clusters with the experimental distributions for related nanoparticles allows one to estimate the reliability of their geometric models proposed based on the results of indirect structural methods.

Small nanoparticles with diameters of 2—5 nm (giant clusters)[127] and related colloidal metal particles of sizes of 5—10 nm occupy a special place among metal nanoclusters. Compounds of this class already exhibit certain physicochemical properties characteristic of bulk metals. However, they are substantially modified by quantum size effects and the influence of the ligand environment.[6b] Since the fraction of metal atoms inside the cluster increases with increasing particle size, up to 40—50% of all atoms are located on the surface of giant clusters, whereas the percentage of such atoms in large nanoparticles with a diameter of ~100 nm is smaller than 1%. Hence, the coordination of surface atoms of a small nanoparticle by ligands

can lead to substantial changes in the properties of the substance. The physical properties of materials consisting of large nanoparticles are modified primarily not by ligands but by the discontinuity of the metal phase and size effects.[6b,122,123]

Usual procedures for the preparation of giant clusters and colloids afford mixtures containing particles with different diameters and stoichiometric compositions, which hinders the complete determination of the structures of nanoclusters from diffraction data.[123,128] Slight variations in the size and composition of nanoparticles are not accompanied by substantial changes in the physicochemical properties of the cluster phase. Hence, in order to grow single crystals, mixtures of particles of similar sizes must be first separated. In the last decade, the chemistry of stoichiometric clusters approaches to small nanoparticles, because several large clusters with a diameter from 1.5 to 6 nm (see Refs. 95—97) were synthesized and studied by X-ray diffraction analysis. These advances give promise that the structure determination of giant clusters at atomic resolution (which is achieved, for example, in X-ray diffraction studies of even larger protein molecules[124]) will be routine. However, X-ray diffraction studies of large clusters are as yet scarce.

Along with the experimental methods of determination of RDF, high-resolution electron microscopy (HREM), scanning tunneling microscopy (STM), small-angle X-ray and neutron scattering (SAXS and SANS, respectively), and spectroscopic methods are also used for studying the structures of nanoclusters. Coherent scattering of X-ray photons on ordered groups of metal atoms in nanoparticles of sizes larger than 1.5—2 nm gives rise to broad reflections in X-ray diffraction patterns, which provide information on the type of atomic packing and interatomic distances (positions of reflections) as well as on the cluster sizes (half-widths of reflections). Hence, the atomic structures of nanoparticles are studied also by powder X-ray diffraction methods and analogous methods based on neutron and electron diffraction.

In this section, we consider selected characteristic examples of structural studies of nanoparticles based on analysis of the experimental radial distribution functions. An analog of RDF (*viz.*, the Fourier transform (FT) magnitude characterized by a shift of the observed coordination spheres to smaller distances *R*) as well as the actual distances to such spheres and their coordination numbers are most often determined by extended X-ray absorption fine structure (EXAFS) spectroscopy.[12.0,125]

It is of interest to compare the coordination spheres, which are revealed for clusters with known structures using EXAFS spectroscopy based on the FT(*R*) dependence, with their radial distribution histograms. The EXAFS studies of the large stoichiometric clusters $Pd_{23}(CO)_{22}(PEt_3)_{10}$ and $Pd_{38}(CO)_{28}(PEt_3)_{12}$, whose molecular structures are considered in Section 3, did not reveal smeared far Pd—Pd
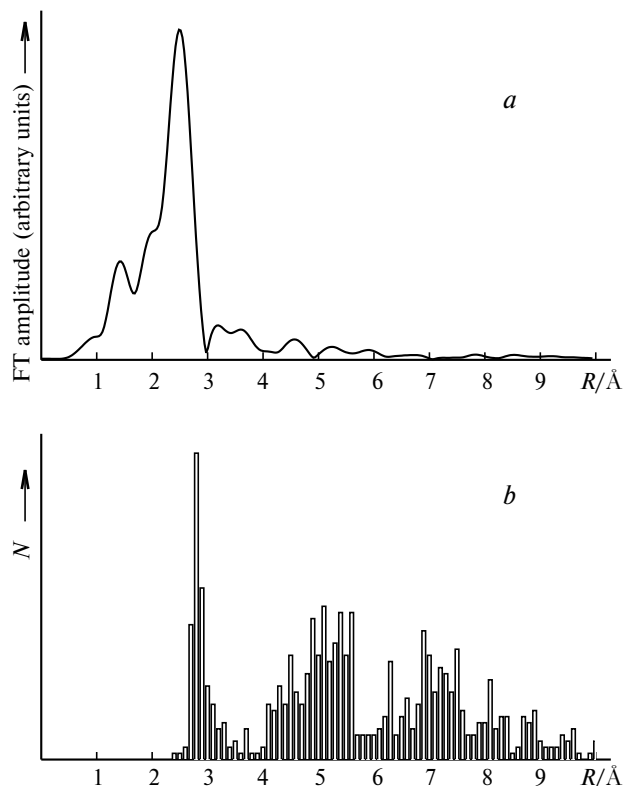
Fig. 18. Metal—metal coordination spheres in the "amorphous" $Pd_{38}(CO)_{28}(PEt_3)_{12}$ cluster[84] (*a*) based on the EXAFS Fourier transform (Pd K-edge) and (*b*) according to the histogram of the Pd—Pd interatomic distances determined by X-ray diffraction analysis.[126]

Table 5. Experimental (EXAFS) Pd—Pd distances (Å) in $Pd_{561}phen_{60}(OAc)_{180}$ and the model Pd—Pd distances for various packing types (see Ref. 127)

EXAFS	f.c.c.	h.c.p.	Icosahedral shells
2.60(4)	2.60	2.60	2.60
3.10(10)	—	—	3.10
3.66(10)	3.67	3.67	3.67
4.08(10)	—	4.24	4.10
—	4.50	4.50	—

coordination spheres, which are observed in the histograms[125,126] (Fig. 18). In EXAFS studies, broad coordination spheres are hidden by their statistical disorder, which impairs photoelectron diffraction and reduces the X-ray absorption fine structure. For this reason, the sizes of metal cores directly found by the EXAFS method from the distances to the last far peak observed in FT are substantially underestimated. Much better estimates of the average sizes of the coherence region, *i.e.*, ordered structural fragments in nanoparticles, can be obtained from the widths of X-ray reflections. The radial atomic distribution functions can be reliably evaluated based on the angular dependence of the X-ray scattering background.[121]

In 1985, the giant palladium cluster with a diameter of ~2.5 nm stabilized by organic ligands was first reliably characterized by physical methods,[127] and its idealized composition, *viz.*, $Pd_{561}phen_{60}(OAc)_{180}$ (phen is 1,10-phenanthroline), was determined. This cluster, which was synthesized by reduction of Pd^{II} salts with hydrogen in an AcOH medium in the presence of the corresponding ligand, is readily soluble in polar organic media (for example, in acetonitrile), but it does not crystallize from these media. The Pd—Pd distances to the nearest coordination spheres of the Pd atoms in this cluster (2.6, 3.1,

3.66, and 4.08 Å) were determined by EXAFS spectroscopy (Table 5). Based on the EXAFS data, the authors of the cited study[127] proposed the geometry of the five-shell Mackay icosahedron composed of 309 interstitial metal atoms and 252 atoms in the outer ν_5-icosahedral shell for this cluster. More recently, giant palladium and platinum clusters, which are characterized by a flexible packing of metal atoms and are readily rearranged under the influence of the ligand environment, were studied.[128]

Reduction of Pt^{II} acetate under analogous conditions afforded colloidal nanoparticles with a different composition, *viz.*, $[Pt_4(phen)(OAc)_3O]_n$, and with a much less ordered local structure.[129] Although according to the SAXS data, the sizes of the metal cores of such particles are ~3.0 nm, only two closest Pt coordination spheres, *viz.*, Pt—O (1.98(1) Å) and Pt—Pt (2.68(3) Å), were revealed in FT EXAFS. Partial oxidation of the resulting Pt colloids is consistent with the X-ray absorption near-edge structure (XANES), which has a pronounced "white" line of the photoelectron transition to the unoccupied 5d-AO. Disorder of the local atomic structure also hides far coordination spheres in the products of thermal aggregation of the resulting colloids, which (according to the data from XANES) are more similar to bulk platinum metal (Fig. 19).[125] Therefore, the EXAFS method imposes additional limitations on the structural data on nanoparticles available in experimental radial distribution functions (Fourier transforms).

The study[127] was followed by the syntheses[130,131] of the related giant Pd and Pt clusters with phenanthroline derivatives as ligands. Based on the electron microscopy data, these compounds were described as imperfect fragments of the f.c.c. packing. According to the HREM data, the $Pt_{309}phen^*_{36}O_{30\pm10}$ cluster (phen* is the disulfonated phenanthroline ligand with composition $(p-C_6H_4SO_3Na)_2C_{12}H_6N_2)$ can be described as a four-shell cuboctahedron.[130] The idealized metal core of this cluster with a diameter of 1.8 nm is characterized by the f.c.c. packing of Pt atoms and has 147 interstitial metal atoms.

The five-shell $Pd_{561}phen_{36}O_{200\pm10}$ cluster with the assumed f.c.c. packing of the metal atoms and phenanthroline ligands was synthesized by G. Schmid and coworkers in a yield of lower than 10%. Analysis of the
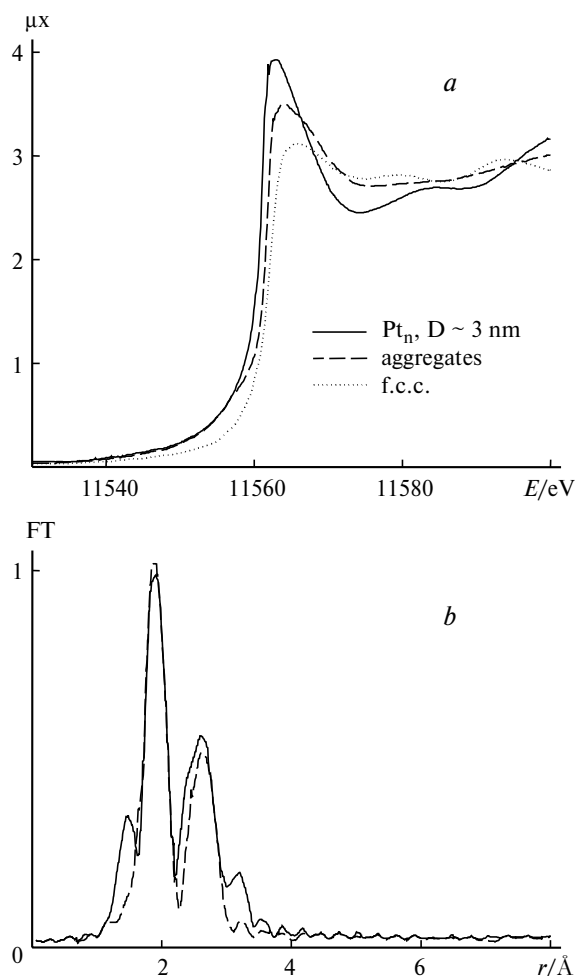
Fig. 19. Profile of the Pt L_{III}-absorption edge for platinum nanoclusters (*a*) and the EXAFS Fourier transforms (*b*; the results of modeling are shown by a dashed line).[129]

other reaction products revealed the $Pd_{1415}phen_{60}O_{\sim 1100}$ (30% yield) and $Pd_{2057}phen_{84}O_{\sim 1600}$ (62% yield) clusters. The compositions and structures of the clusters were determined by electron microprobe analysis, HREM, and powder X-ray diffraction.[131] The $Pd_{1415}phen_{60}O_{\sim 1100}$ cluster with a diameter of 3.2 nm and the $Pd_{2057}phen_{84}O_{\sim 1600}$ cluster with a diameter of 3.6 nm consist, correspondingly, of seven and eight layers of the cubic closest packing with structural defects.

Oxidative aggregation of medium-sized and large Pd carbonyl phosphine clusters in solution, which proceeds through elimination of the PR_3 ligands, affords precipitates of palladium blacks. The latter were also studied by powder X-ray diffraction and EXAFS.[132] Modeling of X-ray diffraction patterns showed that these palladium blacks contain six-shell f.c.c.-type palladium nanoparticles of the idealized formula $Pd_{923}(CO)_xO_y$. According to the results of chemical analysis, these particles retain up to 50% of the carbonyl ligands present in the starting stoichiometric compounds (Fig. 20). The outer Pd—Pd coordination spheres in these nanoparticles revealed by EXAFS are less pronounced than those in the bulk metal due to distortion of the packing under the influence of the ligands (edge effects).

The reliability of structural data can be improved by measuring EXAFS on several elements involved in nanoparticles. For example, chemosorption of Se as a probe on the surface of large f.c.c.-type Ni nanoclusters with a diameter of ~50 nm revealed that these particles have the exposed crystallographic faces (111), whose atomic structure is consistent with the observed Se—Ni distances (2.36 and 3.92 Å).[133] Monitoring of oxidation of the bimetallic cluster anion $[Ni_{32}Au_6(CO)_{44}]^{6-}$ (see Table 3)[85] in an acetonitrile solution by Ni K-edge and
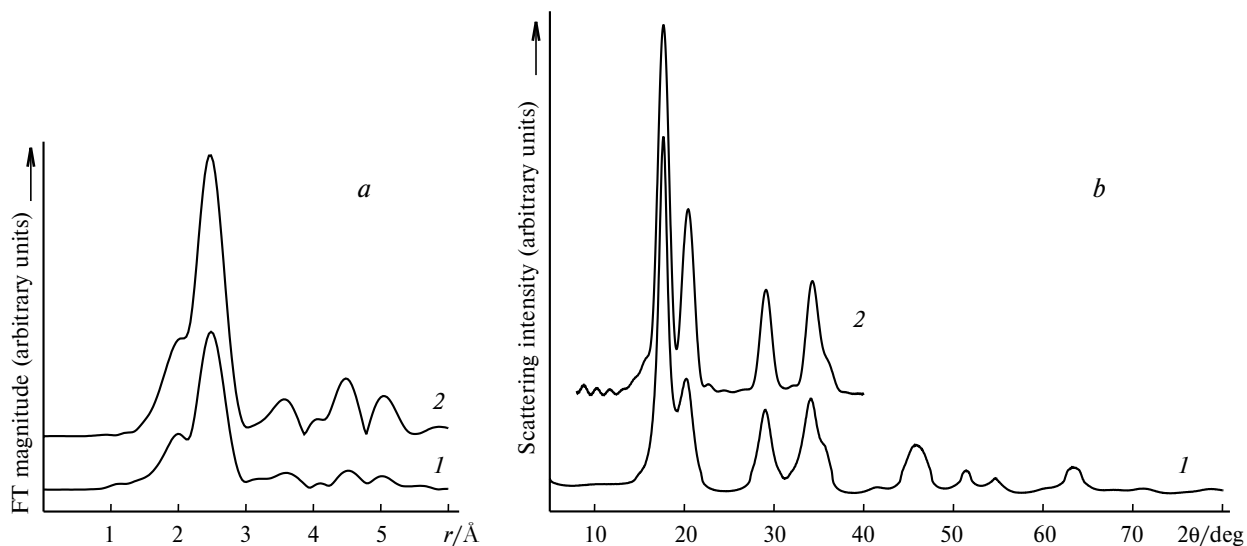

Fig. 20. (*a*) Coordination spheres in the Fourier transforms of Pd K-edge EXAFS for palladium black (*1*) and Pd foil (*2*); (*b*) X-ray diffraction pattern of Pd black (Photon Factory, BL-1B, $\lambda = 0.6888$ Å):[132] *1*, the experimental pattern; *2*, the pattern calculated for the six-shell f.c.c. Pd_{923} cluster.
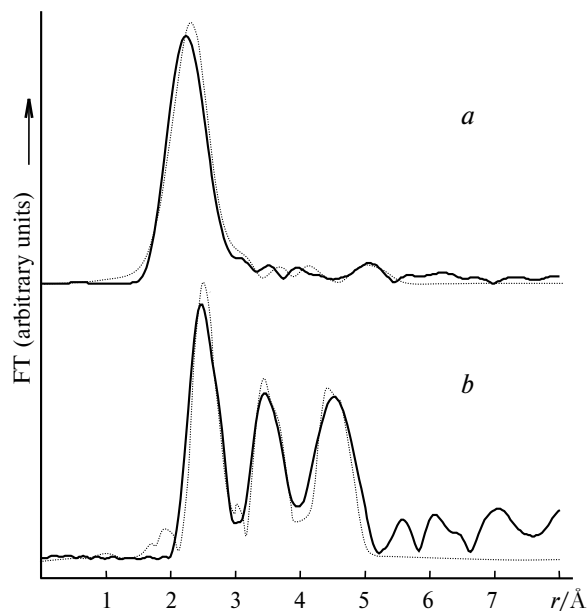
Fig. 21. Coordination spheres in the Fourier transforms of Au L_{III}-edge EXAFS of the $[Au_6Ni_{32}(CO)_{44}]^{6-}$ cluster (*a*)[85] and the product of its oxidation in an acetonitrile solution (*b*). The experimental data and the results of modeling are indicated by solid and dotted curves, respectively. The distances to the metal—metal coordination spheres in the initial cluster/Å according to the EXAFS data (X-ray diffraction data[85] are given in brackets): Ni—Ni, 2.45 [2.48]; Ni—Au, 2.74 [2.68]; Au—Ni, 2.64 [2.68] and 3.76 [3.79]; Au—Au, 2.92 [2.89] and 4.05 [4.07]; in the oxidation product (coordination numbers are given in parentheses): Au—Au, 2.70 Å (4.0), 3.59 Å (10), and 4.58 Å (16); Au—Ni, 2.75 Å (1.5), 3.67 Å (2.0), and 4.67 Å (3.8).

Au L_{III}-edge EXAFS spectroscopy demonstrated the formation of NiO and bimetallic Au/Ni nanoparticles containing the inner core consisting of gold atoms with a packing other than f.c.c. (Fig. 21).[134]

The reconstruction of partial radial distribution functions for atoms of a particular element based on the anomalous X-ray scattering data (see Ref. 121), although being less frequently used, holds considerable promise as an alternative to EXAFS spectroscopy. Studies using this method, which is less sensitive to disorder, revealed, for example, the outer Pt—Pt coordination spheres (6—7 Å) in the partially oxidized supported Pt catalyst (Fig. 22).[135] A comparison of the experimental powder X-ray diffraction patterns with the calculated patterns of model atomic aggregations also holds considerable promise (see, for example, Ref. 132), because one-dimensional diffraction patterns are much more sensitive to atomic packings than RDF. Recent studies[136] of gold nanoparticles with a diameter of ~1.7 nm stabilized by the RS thiolate ligands demonstrated that the experimental X-ray diffraction pattern is in good agreement with the model Au_{145} cluster isostructural to the stoichiometric 145-nuclear palladium cluster prepared by Dahl and co-workers[97] (see above).
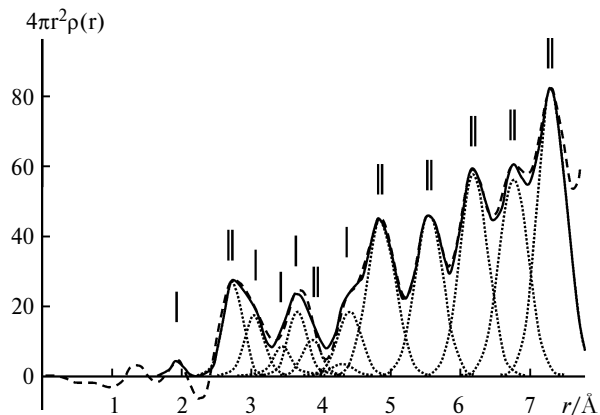
Fig. 22. Coordination spheres of PtO (vertical bars) and Pt (double vertical bars) in the RDF of nanoparticles of the supported EuroPt-1 catalyst ($D \approx 2$—3 nm, HREM) based on the data from anomalous scattering on platinum. The experimental data are indicated by a dashed line; the fitting data are shown by a solid line; the coordination spheres are indicated by dots. The Pt—Pt distances coincide with the f.c.c. metal spheres to within 0.01—0.04 Å.[135]

In the present review, we surveyed only selected studies of the structures of small metal nanoparticles, which attract great interest throughout the world due to their unusual physical characteristics and application in catalysis. Of the voluminous literature devoted to this line of investigation, mention may be made of the studies of the colloidal particles of noble metals,[137—139] highly reactive Ti [140] and Mn nanoclusters[141] of the general formula $[M(THF)_x]_n$ ($x \leq 0.5$), which were prepared by reduction of organometallic compounds, and bimetallic colloidal Pt/Ru particles.[142] In all the cited studies, analysis of RDF (FT) obtained by EXAFS spectroscopy made it possible to determine the distances from the metal atoms to the closest coordination spheres and, in some cases, to reveal the packing mode using other physical methods (see also the reviews[137,138,143] and references cited therein).

5. Conclusion

The development of synthetic methods of cluster chemistry and improvement of X-ray diffraction methods in the last decades made it possible to prepare single crystals of large stoichiometric metal clusters directly related to nanoparticles and to study their crystal structures at atomic resolution. In these large clusters, only several metal atoms are generally located inside the polyhedron, whereas all other atoms are located on the surface of the metal core and are coordinated by ligands. The balance between the energy of interatomic interactions in clusters and the energy of binding of the ligand environment to the cluster core gives rise to various close atomic packings in compounds of this type.

The overview of the X-ray diffraction data for large stoichiometric clusters shows that the latter have frag-

ments of close packings of metal atoms, among which are both crystallographic (f.c.c., h.c.p., b.c.c.) and local packings with the pentagonal symmetry. Analysis of these packings using radial distribution histograms calculated from crystal structures allows one to reveal distortions of ideal packings and the occurrence of mixed (f.c.c./h.c.p., icosahedron—pentagonal prisms) and strongly distorted "amorphous" structures. Homoatomic metal cores of the f.c.c. and h.c.p. types are characterized by either retention or a slight increase in the metallic radii, whereas the shortest interatomic distances in clusters with the icosahedral, "amorphous," or b.c.c. packings vary over a wide range. In some clusters with the pentagonal local symmetry, interstitial atoms are "contracted" and the corresponding metal—metal distances are shortened by 0.1—0.2 Å. In bimetallic clusters formed by metals with different atomic radii, larger metal atoms are generally "contracted" and smaller metal atoms are "expanded." The insertion of nonmetal atoms into large clusters increases distortions of the packing.

For small nonstoichiometric nanoparticles with a diameter of 2—5 nm (giant clusters), which do not form single crystals, the radial distribution functions are determined experimentally by X-ray diffraction and EXAFS spectroscopy. In this case, single-crystal X-ray diffraction data for stoichiometric large clusters enable one to choose the atomic model for nanoparticles and estimate the reliability of conclusions about the atomic structures of clusters based on the results of the above-mentioned methods. In the nearest decade, studies should be, apparently, aimed at synthesizing stoichiometric giant clusters containing comparable fractions of interstitial and exopolyhedral metal atoms in cluster polyhedra and studying these clusters by single-crystal X-ray diffraction in combination with indirect structural methods.

References

1. C. R. Henry, *Appl. Surf. Sci.*, 2000, **164**, 252.
2. S. Bhaduri, *Curr. Sci.*, 2000, **78**, 1318.
3. W. Wernsdorfer, *Met. Clusters Surf.*, 2000, 211.
4. G. Longoni, A. Ceriotti, M. Marchionna, and G. Piro, *Nato ASI Ser., Ser. C*, 1988, **231** (*Surf. Organomet. Chem.: Mol. Approaches Surf. Catal.*), 157.
5. D. Gatteschi and R. Sessoli, *ACS Symp. Ser.*, 1996, **644** (*Molecule-Based Magnetic Materials*), 157.
6. (a) G. Schmid, *Chem. Rev.*, 1992, **92**, 1709; (b) Ya. Volokitin, J. Sinzig, L. J. de Jongh, G. Schmid, M. N. Vargaftik, and I. I. Moiseev, *Nature*, 1996, **384**, 621.
7. J. Jortner, U. Even, A. Goldberg, I. Schek, T. Raz, and R. D. Levine, *Surf. Rev. Lett.*, 1996, **3**, 263.
8. B. K. Teo and H. Zhang, *Polyhedron*, 1990, **9**, 1985.
9. D. M. P. Mingos, *J. Chem. Soc., Chem. Commun.*, 1985, 1352.
10. *Chemistry, Structure and Bonding in Zintl Phases and Ions*, Ed. M. S. Kauzlarich, VCH, Weinheim, 1996,
11. A. F. Wells, *Structural Inorganic Chemistry*, 5th ed., Clarendon Press, Oxford, 1986.
12. S. A. Magarill, N. V. Pervukhina, S. V. Borisov, and N. A. Pal´chik, *Kristallokhimiya soedinenii nizkovalentnoi rtuti* [*Crystal Chemistry of Low-Valent Mercury Compounds*], Yanus-K, Moscow, 2001 (in Russian).
13. Yu. N. Petrov, *Fizika malykh chastits* [*Physics of Small Particles*], Nauka, Moscow, 1982 (in Russian).
14. M. R. Hoare and P. Pal, *Adv. Phys.*, 1971, **20**, 161.
15. V. V. Nauchitel and A. I. Pertsin, *Mol. Phys.*, 1980, **40**, 1341.
16. B. W. van de Waal, G. Torchet, and M.-F. de Feraudy, *Chem. Phys. Lett.*, 2000, **331**, 57.
17. T. Ikeshoji, G. Torchet, M.-F. de Feraudy, and K. Koga, *Phys. Rev. E*, 2001, **63**, 031101.
18. S. P. Gubin, *Khimiya klasterov. Osnovy klassifikatsii i stroenie* [*Chemistry of Clusters. Fundamentals of Classification and Structures*], Nauka, Moscow, 1987 (in Russian).
19. *Physics and Chemistry of Metal Cluster Compounds*, Ed. L. J. de Jongh, Kluwer, Dodrecht, 1994.
20. J. H. Fendler, *Nanoparticeles and Nanostructured Films*, Wiley, Weinheim, 1998.
21. A. P. Alivisatos, *Mat. Res. Soc. Bull.*, 1998, **23**, 18.
22. P. Chini, *J. Organometal. Chem.*, 1980, **200**, 37.
23. P. Chini, G. Longoni, and V. G. Albano, *Adv. Organometal. Chem.*, 1976, **14**, 285.
24. V. G. Albano, G. Ciani, S. Martinengo, and S. Sironi, *J. Chem. Soc., Dalton. Trans.*, 1979, 978.
25. M. Kappes, *Chem. Rev.*, 1988, **88**, 369.
26. M. A. Marcus, M. P. Andrews, J. Zegenhagen, A. S. Bommannavar, and P. Montano, *Phys. Rev.*, 1990, **B42**, 3312.
27. K. Wade, *Chem. Commun.*, 1971, 792.
28. K. Wade, in *Transition Metal Clusters*, Ed. B. F. G. Johnson, Wiley, Chichester, 1980, p. 195.
29. B. K. Teo and N. J. A. Sloane, *Inorg. Chem.*, 1985, **24**, 4545.
30. J. F. Halet, *Coord. Chem. Rev.*, 1995, **635**, 637.
31. Yu. T. Struchkov, A. S. Batsanov, and Yu. L. Slovokhotov, *Sov. Sci. Rev. B. Chem.*, 1987, **10**, 385.
32. U. Simon and G. Schön, in *Handbook of Nanostructured Materials and Nanotechnology*, Ed. H. S. Nalwa, Acad. Press, New York, 2000, **3**, 131.
33. *Chemist´s Handbook*, 3d Ed., Khimiya, Leningrad, 1971, **1**, p. 341 (in Russian).
34. A. L. Patterson and J. S. Kasper, in *International Tables for X-ray Crystallography*, Kluwer, Dodrecht, 1989, **2**, p. 342.
35. Yu. L. Slovokhotov and I. S. Neretin, *Dokl. Akad. Nauk SSSR, Ser. Fiz. Khim.*, 2002, **384**, 216 [*Dokl. Phys. Chem.*, 2002 (Engl. Transl.)].
36. A. L. Makkay, *Acta Cryst.*, 1962, **15**, 916
37. N. A. Bul´enkov and D. L. Tytik, *Izv. Akad. Nauk, Ser. Khim.*, 2001, 1 [*Russ. Chem. Bull., Int. Ed.*, 2001, **50**, 1].

38. H. Krautscheid, D. Fenske, G. Baum, and M. Semmelmenn, *Angew. Chem., Int. Ed. Engl.*, 1993, **32**, 1303.
39. D. Fenske and T. Langtepe, *Angew. Chem., Int. Ed. Engl.*, 2002, **41**, 300.
40. A. Müller, E. Beckmann, H. Bögge, M. Schmidtmann, and A. Press, *Angew. Chem., Int. Ed. Engl.*, 2002, **41**, 1162.
41. D. Washechek, E. J. Wucherer, L. F. Dahl, A. Ceriotti, G. Longoni, M. Manassero, M. Sansoni, and P. Chini, *J. Am. Chem. Soc.*, 1979, **101**, 6110.
42. L. H. Gade, B. F. G. Johnson, J. Lewis, M. McPartlin, H. R. Powell, P. R. Raithby, and W. T. Wong, *J. Chem. Soc., Dalton Trans.*, 1994, 521.
43. M. Kawano, J. W. Bacon, C. F. Campana, B. E. Winger, J. D. Dudek, S. A. Sirchio, S. L. Scruggs, U. Geiser, and L. F. Dahl, *Inorg. Chem.*, 2001, **40**, 2554.
44. L. H. Gade, B. F. G. Johnson, J. Lewis, G. Conole, and M. McPartlin, *J. Chem. Soc., Dalton Trans.*, 1992, 3249.
45. E. Charalambous, L. H. Gade, B. F. G. Johnson, T. Kotch, A. J. Lees, J. Lewis, and M. McPartlin, *Angew. Chem., Int. Ed. Engl.*, 1990, **29**, 1137.
46. L. H. Gade, B. F. G. Johnson, J. Lewis, M. McPartlin, and H. R. Powell, *Chem. Commun.*, 1990, 110.
47. V. G. Albano, F. Calderoni, M. C. Iapalucci, G. Longoni, M. Monari, and P. Zanello, *J. Cluster Sci.*, 1995, **6**, 107.
48. V. G. Albano, L. Grossi, G. Longoni, M. Monari, S. Mulley, and A. Sironi, *J. Am. Chem. Soc.*, 1992, **114**, 5708.
49. K. F. Yung and W. T. Wong, *Angew. Chem., Int. Ed. Engl.*, 2003, **42**, 553.
50. S. Y. W. Hung and W. T. Wong, *Chem. Commun.*, 1997, 2099
51. S. Martinengo, G. Ciani, and A. Sironi, *J. Am. Chem. Soc.*, 1980, **102**, 7564.
52. A. Fumagalli, S. Martinengo, G. Ciani, N. Masciocchi, and A. Sironi, *Inorg. Chem.*, 1992, **31**, 336.
53. J. L. Vidal, R. C. Schoering, and J. M. Troup, *Inorg. Chem.*, 1981, **20**, 227.
54. S. Martinengo, G. Ciani, and A. Sironi, *Chem. Commun.*, 1992, 1405.
55. E. G. Mednikov, N. K. Eremenko, Yu. L. Slovokhotov, and Yu. T. Struchkov, *J. Organomet. Chem.*, 1986, **301**, 35.
56. E. G. Mednikov, N. K. Eremenko, Yu. L. Slovokhotov, and Yu. T. Struchkov, *Zh. Vsesoyuz. Khim. Obshch. im. D. I. Mendeleeva*, 1987, **32**, 101 [*Mendeleev Chem. J.*, 1987 (Engl. Transl.)].
57. C. Femoni, M. C. Iapalucci, G. Longoni, and P. H. Svensson, *Chem. Commun.*, 2001, 1776.
58. J. D. Roth, G. J. Lewis, L. K. Safford, X. Jiang, L. F. Dahl, and M. J. Weaver, *J. Am. Chem. Soc.*, 1992, **114**, 6159.
59. B. K. Teo, H. Zhang, and X. Shi, *Inorg. Chem.*, 1994, **33**, 4086.
60. B. K. Teo, H. Zhang, and X. Shi, *J. Am. Chem. Soc.*, 1993, **115**, 8489.
61. T. G. M. M. Kappen, P. P. J. Schlebos, J. J. Bour, W. P. Bosman, J. M. M. Smits, P. T. Beurskens, and J. J. Steggerda, *Inorg. Chem.*, 1994, **33**, 754.
62. B. K. Teo and H. Zhang, *Coord. Chem. Rev.*, 1995, **143**, 611.
63. B. K. Teo and H. Zhang, *Inorg. Chem.*, 1991, **30**, 3115.
64. B. K. Teo, X. Shi, and H. Zhang, *J. Cluster Sci.*, 1993, **4**, 471.
65. B. K. Teo and H. Zhang, *Angew. Chem., Int. Ed. Engl.*, 1992, **31**, 445.
66. H. M. Chun, H. Z. Ying, C. Rong, J. F. Long, and L. H. Qin, *Chinese J. Struct. Chem. (Jiegou Huaxue)*, 1993, **12**, 334.

67. B. K. Teo, H. Zhang, and X. Shi, *Inorg. Chem.*, 1990, **29**, 2083.
68. B. K. Teo, X. Shi, and H. Zhang, *J. Am. Chem. Soc.*, 1991, **113**, 4329.
69. B. K. Teo, X. Shi, and H. Zhang, *Chem. Commun.*, 1992, 1195.
70. M. A. Beswick, J. Lewis, P. R. Raithby, and M. C. Ramirez de Arellano, *Angew. Chem., Int. Ed. Engl.*, 1997, **36**, 2227.
71. N. T. Tran, M. Kawano, D. R. Powell, and L. F. Dahl, *J. Chem. Soc., Dalton Trans.*, 2000, 4138.
72. A. Fumagalli, S. Martinengo, G. Bernasconi, G. Ciani, D. M. Proserpio, and A. Sironi, *J. Am. Chem. Soc.*, 1997, **119**, 1450.
73. E. G. Mednikov, S. A. Ivanov, and L. F. Dahl, *Angew. Chem., Int. Ed. Engl.*, 2003, **42**, 323.
74. C. Femoni, M. C. Iapalicci, G. Longoni, P. H. Svensson, and J. Wolowska, *Angew. Chem., Int. Ed. Engl.*, 2000, **39**, 1635.
75. N. T. Tran, M. Kawano, and L. F. Dahl, *J. Chem. Soc., Dalton Trans.*, 2001, **19**, 2731.
76. E. G. Mednikov and N. I. Kanteeva, *Izv. Akad. Nauk, Ser. Khim.*, 1995, 167 [*Russ. Chem. Bull.*, 1995, **44**, (Engl. Transl.)].
77. A. Ceriotti, A. Fait, G. Longoni, G. Piro, L. Resconi, F. Demartin, M. Manassero, N. Masciocchi, and M. Sansoni, *J. Am. Chem. Soc.*, 1986, **108**, 5370.
78. C. Femoni, M. C. Iapalucci, G. Longoni, and P. H. Svensson, *Chem. Commun.*, 2000, 655.
79. P. D. Mlynek, M. Kawano, M. A. Kozee, and L. F. Dahl, *J. Cluster Sci.*, 2001, **12**, 313.
80. B. K. Teo, M. Hong, H. Zhang, D. Huang, and X. Shi, *Chem. Commun.*, 1988, 204.
81. B. K. Teo, H. Zhang, and X. Shi, *J. Am. Chem. Soc.*, 1990, **112**, 8552.
82. B. K. Teo, X. Shi, and H. Zhang, *Inorg. Chem.*, 1993, **32**, 3987.
83. B. K. Teo, M. Hong, and H. Zhang, *Angew. Chem., Int. Ed. Engl.*, 1987, **26**, 897.
84. E. G. Mednikov, N. K. Eremenko, Yu. L. Slovokhotov, and Yu. T. Struchkov, *Chem. Commun.*, 1987, 218.
85. N. T. Tran, M. Kawano, D. R. Powell, R. K. Hayashi, C. F. Campana, and L. F. Dahl, *J. Am. Chem. Soc.*, 1999, **121**, 5945.
86. A. Ceriotti, A. Fait, G. Longoni, G. Piro, F. Demartin, M. Manassero, N. Masciocchi, and M. Sansoni, *J. Am. Chem. Soc.*, 1986, **108**, 8091.
87. B. K. Teo, X. Shi, and H. Zhang, *J. Am. Chem. Soc.*, 1992, **114**, 2743.
88. J. Zhang and L. F. Dahl, *J. Chem. Soc., Dalton Trans.*, 2002, **7**, 1269.
89. M. A. Kozee, J. Zhang, and L. F. Dahl, *219th ACS National Meeting, Book of Abstracts*, 2000, INOR-403.
90. F. Demartin, C Femoni, M. C. Iapalucci, G. Longoni, and P. Macchi, *Angew. Chem., Int. Ed. Engl.*, 1999, **38**, 531.
91. J. M. Bemis and L. F. Dahl, *J. Am. Chem. Soc.*, 1997, **119**, 4545.
92. M. Kawano, J. W. Bacon, C. F. Campana, and L. F. Dahl, *J. Am. Chem. Soc.*, 1996, **118**, 7869.
93. A. Ceriotti and G. Longoni, *Angew. Chem., Int. Ed. Engl.*, 1985, **24**, 697.
94. J. D. Roth, G. J. Lewis, L. K. Safford, X. Jiang, and L. F. Dahl, *J. Am. Chem. Soc.*, 1992, **114**, 6159.

95. D. Fenske and F. Simon, *Angew. Chem., Int. Ed. Engl.*, 1997, **36**, 230.
96. N. T. Tran and L. F. Dahl, *Angew. Chem., Int. Ed. Engl.*, 2003, **42**, 3533.
97. N. T. Tran, D. R. Powell, and L. F. Dahl, *Angew. Chem., Int. Ed. Engl.*, 2000, **39**, 4121.
98. G. Schmid, R. Pfeil, R. Boese, F. Bandermann, S. Meyer, G. H. M. Calis, and J. V. A. van der Velden, *Chem. Ber.*, 1981, **114**, 3634.
99. G. Schmid, U. Giebel, and W. Huster, *Inorg. Chim. Acta*, 1984, **85**, 97.
100. G. Schmid and W. Huster, *Naturforsch.*, 1986, **41b**, 1028.
101. R. W. Broach, L. F. Dahl, G. Longoni, P. Chini, A. J. Schultz, and J. M. Williams, *Adv. Chem. Ser.*, 1978, **167**, 93.
102. A. F. Wells, *Structural Inorganic Chemistry*, 5th ed., Clarendon Press, Oxford, 1986.
103. S. Martinengo, G. Ciani, A. Sironi, and P. Chini, *J. Am. Chem. Soc.*, 1978, **100**, 7096.
104. C. E. Briant, B. R. C. Theobald, J. W. White, L. K. Bell, D. M. P. Mingos, and A. J. Welch, *Chem. Commun.*, 1981, 201.
105. J. W. A. van der Velden, F. A. Vollenbroek, J. J. Bour, P. T. Beurskens, J. M. M. Smits, and W. P. Bosman, *Rec. Trav. Chim. Pays-Bas (Rec. J. R. Neth. Chem. Soc.)*, 1981, **100**, 148.
106. M. Laupp and J. Strahle, *Angew. Chem., Int. Ed.*, 1994, **33**, 207.
107. M. Laupp and J. Strahle, *Z. Naturforsch., B*, 1995, **50**, 1369.
108. R. C. B. Copley and D. M. P. Mingos, *J. Chem. Soc., Dalton Trans.*, 1996, **491**.
109. R. C. B. Copley and D. M. P. Mingos, *J. Chem. Soc., Dalton Trans.*, 1992, 1755.
110. E. G. Mednikov, Yu. L. Slovokhotov, and Yu. T. Struchkov, *Metalloorg. Khim.*, 1991, **4**, 123 [*Organomet. Chem. USSR*, 1991, **4** (Engl. Transl.)].
111. S. S. Kurasov, N. K. Eremenko, Yu. L. Slovokhotov, and Yu. T. Struchkov, *J. Organomet. Chem.*, 1989, **361**, 405.
112. V. G. Albano, P. Chini, S. Martinengo, M. Sansoni, and D. Strumolo, *J. Chem. Soc., Dalton Trans.*, 1976, 970.
113. D. Levine and P. J. Steinhardt, *Phys. Rev. B*, 1986, **34**, 596.
114. C. Janot, *Quasicrystals. A Primer*, 2nd ed., Clarendon, Oxford, 1995.
115. *Physics of Simple Liquids*, Eds. H. N. V. Temperley, J. S. Rowlinson, and G. S. Rushbrooke, North-Holland, Amsterdam, 1968.
116. Yu. L. Slovokhotov and Yu. T. Struchkov, *Usp. Khim.*, 1985, **54**, 556 [*Russ. Chem. Rev.*, 1985, **54** (Engl. Transl.)].
117. H. M. Lee, M. M. Olmstead, T. Suetsuna, H. Shimotani, N. Dragoe, R. J. Cross, K. Kitazawa, and A. L. Balch, *Chem. Commun.*, 2002, 1352.
118. M. M. Olmstead, A. de Bettencourt-Dias, J. C. Duchamp, S. Stevenson, H. C. Dorn, and A. L. Balch, *J. Am. Chem. Soc.*, 2000, **122**, 12220.
119. P. J. M. W. L. Birker, J. Reedijk, and G. O. Verschoor, *Inorg. Chem.*, 1981, **20**, 2877.
120. *Rentgenospektral´nyi metod izucheniya struktury amorfnykh tel. EXAFS-spektroskopiya* [*X-ray Spectral Method for Investigation of the Structure of Amorphous Solids. EXAFS Spectroscopy*], Ed. G. M. Zhidomirov, Nauka, Novosibirsk, 1988 (in Russian).
121. E. M. Moroz, *Usp. Khim.*, 1991, **61**, 356 [*Russ. Chem. Rev.*, 1991, **61** (Engl. Transl.)].
122. *Clusters and Colloids, from Theory to Applications*, Ed. G. Schmid, VCH, Weinheim, 1994.
123. L. G. de Jongh, *Applied Organometallic Chemistry*, 1998, **12**, 393.
124. *Strukturnye issledovaniya kristallov (Ser. Problemy sovremennoi kristallokhimii)* [*Structural Studies of Crystals (Ser. Problems of Modern Crystallography)*], Ed. V. I. Simonov, Nauka, Fizmatlit, Moscow, 1996 (in Russian).
125. Yu. L. Slovokhotov, in *Solid State Organometallic Chemistry: Methods and Applications*, Eds. M. Gielen, R. Willem, and B. Wrackmeyer, Wiley, Chichester, 1999, p. 113.
126. O. A. Belyakova, Y. V. Zubavichus, and Yu. L. Slovokhotov, *Nucl. Instr. Meth. Phys. Res. A*, 2000, **448**, 302.
127. M. N. Vargaftik, V. P. Zagorodnikov, I. P. Stolyarov, I. I. Moiseev, V. I. Likholobov, D. I. Kochubey, A. L. Chuvilin, V. I. Zaikowsky, K. L. Zamaraev, and G. I. Timofeeva, *Chem. Commun.*, 1985, 937.
128. (a) M. N. Vargaftik, I. I. Moiseev, D. I. Kochubey, and K. L. Zamaraev, *Faraday Discuss.*, 1991, **92**, 13; (b) I. I. Moiseev and M. N. Vargaftik, *New J. Chem.*, 1998, 1217.
129. B. N. Novgorodov, D. I. Kochubey, and M. N. Vargaftik, *Nucl. Instr. Meth. Phys. Res. A*, 1998, **405**, 351.
130. G. Schmid, B. Morun, and J.-O. Malm, *Angew. Chem., Int Engl.. Ed.*, 1989, **28**, 778.
131. G. Schmid, M. Harms, J.-O. Malm, J.-O. Bovin, J. van Ruitenbeck, H. W. Zandbergen, and W. T. Fu, *J. Am. Chem. Soc.*, 1993, **115**, 2046.
132. O. A. Belyakova, E. G. Mednikov, P. V. Petrovskii, Yu. L. Slovokhotov, I. Kubozono, and S. Kashino, *Tez. dokl., XIV Ross. konf. po ispol´zovaniyu sinkhrotronnogo izlucheniya (SI-2002)* [*Abstrs. of Papers, XIV Russian Conf. on Use of Synchrotron Radiation (SR-2002)*], Novosibirsk, 2002, p. 46 (in Russian).
133. V. V. Kriventsov, B. N. Novgorodov, and D. I. Kochubey, *Nucl. Instr. Meth. Phys. Res. A*, 1998, **405**, 382.
134. O. A. Belyakova, Y. Kubozono, S. Kashino, and Yu. L. Slovokhotov, *Physica Scripta*, 2003, in press.
135. A. N. Shmakov, E. M. Moroz, and A. L. Chuvilin, *Nucl. Instr. Meth. Phys. Res. A*, 1998, **405**, 470.
136. T. G. Schaaff, M. Shafigullin, J. T. Khoury, I. Vezmar, and R. L. Wetten, *J. Phys. Chem.*, 2001, **105**, 8785.
137. I. I. Moiseev and M. N. Vargaftik, in *Catalysis by Di- and Polynuclear Metal Cluster Complexes*, Eds. R. D. Adams and F. A. Cotton, Wiley-VCH, New York, 1998, p. 395.
138. L. N. Lewis, *Chem. Rev.*, 1993, **64**, 1449.
139. T. Fujimoto, A. Fukuoka, S. Iijima, and M. Ichikawa, *J. Phys. Chem.*, 1993, **97**, 279.
140. H. Boneman and B. Korall, *Angew. Chem., Int. Ed. Engl.*, 1992, **31**, 1490.
141. R. Franke, J. Rothe, R. Becker, J. Pollmann, J. Hormes, H. Bönnemann, and R. Koppler, *Adv. Mater.*, 1988, **10**, 126.
142. W. Vogel, P. Britz, H. Bönnemann, J. Rothe, and J. Hornes, *J. Phys. Chem.*, 1997, **101**, 11029.
143. *Active Metals: Preparation, Characterisation, Applications*, Ed. A. Fürstner, VCH, Weinheim, 1996.